Allelic Variation of *MYB10* Is the Major Force Controlling Natural Variation in Skin and Flesh Color in Strawberry (*Fragaria* spp.) Fruit[OPEN]

Cristina Castillejo,[a,b] Veronika Waurich,[c,d] Henning Wagner,[c,d] Rubén Ramos,[a,b] Nicolás Oiza,[a,b] Pilar Muñoz,[a,b] Juan C. Triviño,[e] Julie Caruana,[f] Zhongchi Liu,[f] Nicolás Cobo,[g,h] Michael A. Hardigan,[g] Steven J. Knapp,[g] José G. Vallarino,[b,i] Sonia Osorio,[b,i] Carmen Martín-Pizarro,[b,i] David Posé,[b,i] Tuomas Toivainen,[j] Timo Hytönen,[j,k,l] Youngjae Oh,[m] Christopher R. Barbey,[m] Vance M. Whitaker,[m] Seonghee Lee,[m] Klaus Olbricht,[c] José F. Sánchez-Sevilla,[a,b] and Iraida Amaya[a,b,1]

[a] Laboratorio de Genómica y Biotecnología, Instituto Andaluz de Investigación y Formación Agraria y Pesquera (IFAPA) Centro de Málaga, 29140 Málaga, Spain

[b] Unidad Asociada de I + D + i IFAPA-Consejo Superior de Investigaciones Científicas-Universidad de Málaga (IFAPA-IHSM) Biotecnología y Mejora en Fresa, Málaga 29071, Spain

[c] Hansabred GmbH & Co. KG, 01108 Dresden, Germany

[d] Institut für Botanik, Technische Universität Dresden, 01062 Dresden, Germany

[e] Sistemas Genómicos, 46980 Valencia, Spain

[f] Department of Cell Biology and Molecular Genetics, University of Maryland, College Park, Maryland 20742

[g] Department of Plant Sciences, University of California, Davis, California 95616

[h] Departamento de Producción Agropecuaria, Universidad de La Frontera, Temuco 01145, Chile

[i] Departmento de Biología Molecular y Bioquímica, Instituto de Hortofruticultura Subtropical y Mediterránea "La Mayora" (IHSM), Universidad de Málaga-Consejo Superior de Investigaciones Científicas, Campus de Teatinos 29071, Málaga, Spain

[j] Department of Agricultural Sciences, Viikki Plant Science Centre, University of Helsinki, Helsinki 00790, Finland

[k] Organismal and Evolutionary Biology Research Programme, Faculty of Biological and Environmental Sciences, Viikki Plant Science Centre, University of Helsinki, Helsinki 00790, Finland

[l] National Institute of Agricultural Botany East Malling Research (NIAB EMR), Kent ME19 6BJ, United Kingdom

[m] Department of Horticultural Sciences, University of Florida, Institute of Food and Agricultural Sciences (IFAS) Gulf Coast Research and Education Center, Wimauma, Florida 33598

ORCID IDs: 0000-0003-2596-8790 (C.C.); 0000-0002-0055-7787 (V.W.); 0000-0001-5357-4356 (H.W.); 0000-0002-7107-4416 (R.R.); 0000-0003-4929-4057 (N.O.); 0000-0003-1673-3009 (P.M.); 0000-0001-6752-8000 (J.C.T.); 0000-0002-3792-371X (J.C.); 0000-0001-9969-9381 (Z.L.); 0000-0001-7433-8117 (N.C.); 0000-0001-6926-7561 (M.A.H.); 0000-0001-6498-5409 (S.J.K.); 0000-0002-0374-8706 (J.G.V.); 0000-0002-0159-6091 (S.O.); 0000-0001-9305-3096 (C.M.-P.); 0000-0003-3332-4661 (D.P.); 0000-0002-2817-8121 (T.T.); 0000-0002-5231-4031 (T.H.); 0000-0002-3230-9753 (Y.O.); 0000-0002-2759-6081 (C.R.B.); 0000-0002-2172-3019 (V.M.W.); 0000-0002-5190-8014 (S.L.); 0000-0003-1124-2585 (K.O.); 0000-0002-6690-7196 (J.F.S.-S.); 0000-0002-4612-8902 (I.A.)

The fruits of diploid and octoploid strawberry (*Fragaria* spp) show substantial natural variation in color due to distinct anthocyanin accumulation and distribution patterns. Anthocyanin biosynthesis is controlled by a clade of R2R3 MYB transcription factors, among which MYB10 is the main activator in strawberry fruit. Here, we show that mutations in *MYB10* cause most of the variation in anthocyanin accumulation and distribution observed in diploid woodland strawberry (*F. vesca*) and octoploid cultivated strawberry (*F.* ×*ananassa*). Using a mapping-by-sequencing approach, we identified a *gypsy*-transposon in *MYB10* that truncates the protein and knocks out anthocyanin biosynthesis in a white-fruited *F. vesca* ecotype. Two additional loss-of-function mutations in *MYB10* were identified among geographically diverse white-fruited *F. vesca* ecotypes. Genetic and transcriptomic analyses of octoploid *Fragaria* spp revealed that *FaMYB10-2*, one of three *MYB10* homoeologs identified, regulates anthocyanin biosynthesis in developing fruit. Furthermore, independent mutations in *MYB10-2* are the underlying cause of natural variation in fruit skin and flesh color in octoploid strawberry. We identified a CACTA-like transposon (*FaEnSpm-2*) insertion in the *MYB10-2* promoter of red-fleshed accessions that was associated with enhanced expression. Our findings suggest that cis-regulatory elements in *FaEnSpm-2* are responsible for enhanced *MYB10-2* expression and anthocyanin biosynthesis in strawberry fruit flesh.

INTRODUCTION

The characteristic red color of strawberry (*Fragaria* spp) fruit is due to the accumulation of anthocyanins. These water-soluble pigments are synthesized through the flavonoid pathway (Almeida et al., 2007; Tohge et al., 2017). The initial substrate, 4-coumaroyl-CoA (CoA), is produced from phenylalanine through the sequential activity of the general phenylpropanoid pathway enzymes phenylalanine ammonia-lyase (PAL), cinnamate 4-hydroxylase (C4H), and 4-coumarate:CoA ligase. The flavonoid pathway begins with

IN A NUTSHELL

Background: The red color of strawberry fruits results from the accumulation of anthocyanins, which are synthesized through the well-known flavonoid pathway. Anthocyanins are synthesized at the endoplasmic reticulum and are later transported into the vacuole for storage via different types of mechanisms. Anthocyanin biosynthesis is induced or repressed through transcriptional regulation of structural genes by transcription factors such as MYB, bHLH, and WD-repeat proteins. A large natural variation in color can be observed in different diploid and octoploid strawberry accessions. Besides contributing to fruit color, anthocyanins possess anti-oxidative properties with beneficial effects on human health.

Question: We wanted to know which genes were responsible for the natural fruit color variation in strawberry. Identification of the genes affecting external (skin) and internal (flesh) fruit color would facilitate the development of molecular markers for the efficient development of new strawberry varieties with increased or reduced levels of anthocyanins.

Findings: We used 12 accessions of diploid strawberry (*F. vesca*) that produce completely white fruits and seven accessions of octoploid strawberry (*F. × ananassa*) differing in skin and/or flesh color and compared them to completely red fruits. We found that all analyzed color variants in the genus *Fragaria* were caused by independent mutations in the same gene, the transcription factor gene *MYB10*. In diploid *Fragaria*, we identified three mutant alleles of *MYB10* (one was previously described) and a large deletion in chromosome 1 that completely removed the gene. In octoploid strawberry, we found that anthocyanin biosynthesis is activated predominantly by *MYB10-2,* one of the three *MYB10* copies present in this polyploid genome. Two independent mutations of *MYB10* were found to be responsible for the white-skin phenotype, while red-flesh color was associated with the presence of a transposon insertion in the *MYB10-2* promoter.

Next steps: Our findings reveal a simple genetic control of *MYB10* over strawberry skin and flesh color, making it a good target for marker-assisted breeding as well as gene editing using CRISPR-Cas9 technology. In the future, we would like to identify which transcription regulatory sequence(s) provided by the transposon inserted at *MYB10-2* promoter drive(s) *MYB10-2* induction in fruit flesh.

the condensation of one molecule of 4-coumaroyl- CoA and three molecules of malonyl-CoA by chalcone synthase (CHS). Chalcone isomerase (CHI) subsequently converts naringenin chalcone into naringenin. The subsequent steps involving flavonoid 3-hydroxylase (F3H) and flavonoid 3′,5′-hydroxylase (F3′5′H) generate dihydro-flavonols. The genes encoding the enzymes involved in these steps are known as early biosynthetic genes. Downstream genes of the pathway are known as late biosynthetic genes. These genes encode dihydroflavonol 4-reductase (DFR), which generate colorless leucoanthocyanidins, anthocyanidin synthase (ANS), which produces anthocyanidins, and several glycosyltransferases (UFGTs) that attach sugar molecules to anthocyanidins to generate the first stable anthocyanins.

Anthocyanins are synthesized at the endoplasmic reticulum and are later transported into the vacuole for storage via different types of mechanisms, including transport via glutathione *S*-transferases (GSTs; Luo et al., 2018). Anthocyanin biosynthesis is tuned through the transcriptional regulation of structural genes by transcription factors including MYB, bHLH, and WD-repeat proteins, which form the MBW ternary complex (Jaakola, 2013; Zhang et al., 2014; Xu et al., 2015). R2R3 MYB transcription factors are often the major determinants of natural variation in anthocyanin

biosynthesis (Allan et al., 2008). In strawberry, the R2R3 MYB10 TF is considered to be the primary activator of structural genes in the anthocyanin pathway during fruit development (Lin-Wang et al., 2010; Medina-Puche et al., 2014), whereas another R2R3 MYB transcription factor from ripening strawberry, FaMYB1, represses the transcription of anthocyanin-related genes (Aharoni et al., 2001; Salvatierra et al., 2013).

Fruit color is a key quality trait for fruit breeders. Fruit color in the genus *Fragaria* varies widely from completely white fruits (WFs) to dark red, with wide variation in the internal concentration and distribution of anthocyanins throughout the fruit (Hancock, 1999; Hancock et al., 2003). Gaining insight into the genetic factors affecting natural variation in external (skin) and internal (flesh) fruit color is crucial for the efficient modification of this trait in new cultivars and will facilitate the rapid development of fruits with increased or reduced levels of anthocyanins. Besides contributing to fruit color, anthocyanins possess anti-oxidative properties, with several health-promoting effects and positive impacts on cardiovascular disorders and degenerative diseases (He and Giusti, 2010; Del Rio et al., 2013; Forbes-Hernandez et al., 2016).

The genus *Fragaria* belongs to the Rosaceae family and comprises 24 species, including the worldwide cultivated strawberry (*Fragaria* ×*ananassa*; Staudt, 2009; Liston et al., 2014). This genus displays a series of ploidy levels, ranging from diploid species such as *Fragaria vesca* (2n=2x=14) to decaploid species such as some accessions of *Fragaria iturupensis* (2n=10x=70). The cultivated strawberry, *Fragaria* ×*ananassa*, originated in France nearly 300 years ago via hybridization between two wild octoploid species, *Fragaria chiloensis* and *Fragaria virginiana*, which were introduced from South and North America, respectively

[1] Address correspondence to iraida.amaya@juntadeandalucia.es.
The author responsible for distribution of materials integral to the findings presented in this article in accordance with the policy described in the Instructions for Authors (www.plantcell.org) is: Iraida Amaya (iraida.amaya@juntadeandalucia.es).

(Darrow, 1966; Hancock, 1999). Cultivated strawberry and its wild progenitor species are allo-polyploids with 2n=8x=56 chromosomes. Recent studies agree that one of the four subgenomes of the octoploid *Fragaria* species originated from a *F. vesca* ancestor and another from a *F. iinumae* ancestor, while the origin of the remaining two subgenomes, possibly related to the extant species *Fragaria viridis* and *Fragaria nipponica*, is still under investigation (Tennessen et al., 2014; Edger et al., 2019, 2020; Liston et al., 2020).

Due to its simpler diploid genome, *F. vesca* is a model for genetic and genomic studies. Efficient genomic resources have been generated for this species, including transcriptomes (Hollender et al., 2012; 2014; Li et al., 2019) and a recently improved near-complete genome sequence (Shulaev et al., 2011; Edger et al., 2018). *F. vesca* accessions with WFs, including the sequenced Hawaii4 accession, have been described and stored in multiple germplasm repositories. Despite having red skin color, *F. vesca* accessions, such as 'Reine des Vallées' or 'Ruegen,' are all characterized by white or pale-yellow flesh (NCGR, Corvallis repository). Red versus white external fruit color in *F. vesca* is governed by a single locus named *C* (Brown and Wareing, 1965). The *c* locus from the 'Yellow Wonder' cultivar was subsequently mapped to the bottom of linkage group (LG) 1 (Williamson et al., 1995; Deng and Davis, 2001). A recent genome-scale variant analysis showed that a single nucleotide polymorphism (SNP; G35C) causing an amino acid change (W12S) in the *FvMYB10* gene was responsible for the loss of anthocyanins and the pale color of 'Yellow Wonder' fruits (Hawkins et al., 2016).

Several studies have focused on characterizing most of the structural and regulatory genes necessary for color development in the genus *Fragaria* (Moyano et al., 1998; Lunkenbein et al., 2006; Griesser et al., 2008; Carbone et al., 2009; Salvatierra et al., 2010; 2013; Thill et al., 2013; Fischer et al., 2014; Lin-Wang et al., 2014; Medina-Puche et al., 2014; Miosic et al., 2014; Duan et al., 2017; Hossain et al., 2018; and references therein). The identification of genes or genomic regions governing fruit color variation in cultivated strawberry is crucial for hastening the development of new cultivars with desired characteristics. However, the octoploid nature of this species complicates genetic analyses because up to eight alleles can be found if each homoeologous locus from the four subgenomes were conserved after polyploidization (Edger et al., 2019). A number of studies have detected quantitative trait loci (QTL) contributing to the external color intensity or anthocyanin content of strawberry fruits (Zorrilla-Fontanesi et al., 2011; Lerceteau-Köhler et al., 2012; Castro and Lewers, 2016). Each of these three studies identified three to six genomic regions that contribute to color-related traits, but the phenotypic variation explained by each QTL was relatively low, with only a few QTLs explaining more than 15% of phenotypic variation.

More recently, an 8-bp insertion in the coding region of *FaMYB10* was associated with the loss of anthocyanins in fruits of cv Snow Princess, an octoploid strawberry cultivar with completely WFs (Wang et al., 2020), but its subgenome location was not described. Three full-length homoeologous *FaMYB10* genes were annotated in the octoploid cv Camarosa genome (Edger et al., 2019). The patterns of expression and roles of these genes in determining fruit color variation are not fully known. Are all three genes mutated in white octoploid strawberry? How many homoeologs are expressed in developing fruit? Natural strawberry fruit color mutants affected in genes other than *MYB10* have not been found. However, strawberry fruit color variants have been obtained by transient downregulation of the anthocyanin biosynthesis repressor *FcMYB1,* resulting in increased concentrations of anthocyanins. In addition, transient knock-down of *RAP*, encoding a GST operating as carrier protein of anthocyanins, led to reduced fruit coloration in cultivated strawberry (Salvatierra et al., 2013; Gao et al., 2020). Are any of these genes, apart from *MYB10*, behind fruit color variations found in nature?

In this study, we performed an extensive phenotypic, genetic, and molecular analysis of *Fragaria* genetic resources to identify genetic determinants that contribute to natural fruit color variation in strawberry. First, we screened available diversity for fruit color in the diploid *F. vesca* and identified new mutations for the loss of anthocyanins and associated red color. We then extended the analysis to seven octoploid accessions with fruit with either white flesh/red skin or white flesh/white skin compared to fruits with red flesh/red skin. One of our objectives was to identify specific alleles in cultivated strawberry that could be targeted for marker development that would aid breeders in the efficient development of new improved cultivars with desired fruit color. Strikingly, our results show that all analyzed color variants in the genus *Fragaria* are caused by independent mutations in the same gene, *MYB10*. Different genetic lesions are responsible for distinct flesh and skin color phenotypes, and therefore, allele-specific markers will need to be developed to track specific traits. We further show that independent mutations in only one of three *MYB10* homoeologs (*MYB10-2*) cause skin- and flesh-color variation in octoploid strawberry. Red-flesh color was linked to a CACTA-like transposon insertion in the *FaMYB10* promoter, while white-flesh mutant alleles lacking this insertion were inherited from white-fleshed *F. chiloensis* donors. We developed a high-resolution melting (HRM) marker able to predict WF skin color derived from a mutation in the coding region of *FaMYB10*. Subsequently, we developed two additional DNA markers, including one based on PCR and agarose gel and another on KASP (Kompetitive allele-specific PCR) that predict internal fruit color in diverse octoploid strawberry germplasm. These markers represent useful tools for the selection of fruit color, particularly when *F. chiloensis* accessions are used in breeding programs.

RESULTS AND DISCUSSION

Identification of Loci Controlling External Fruit Color in *F. vesca*

To identify genetic factors affecting fruit color in *F. vesca*, we developed an F_2 mapping population of 145 lines derived from cv Reine des Vallées (RV660) and the IFAPA white-fruited accession ESP138.596 (WV596). As previously described for other backgrounds (Brown and Wareing, 1965), red versus WF color in the RV660 × WV596 F_2 population segregated as expected for a single mutation (1:3; χ^2 test, P = 0.922). To fast-map the locus controlling red color in this *F. vesca* population, we prepared two pools and subjected them to a QTL-Seq approach (Takagi et al., 2013) that combines bulk-segregant analysis (Michelmore et al.,

1991) with NGS technologies to locate candidate genomic regions more rapidly than traditional linkage mapping. We selected 34 F_2 plants with red fruits (RFs) and 32 F_2 plants with WFs to generate the two DNA pools referred to as RF and WF, respectively. Next, we performed Illumina high-throughput sequencing of each pool to a 50× genome coverage and aligned short reads to the *F. vesca* reference genome v4.0.a1 (Edger et al., 2018). Frequencies for SNPs in each pool were calculated, and average SNP-indexes were computed in 3-Mb intervals. The difference in SNP allele frequencies between the RF and WF pools (ΔSNP-index) were plotted against the *F. vesca* genome (Figure 1A). At the 97% confidence level, significant SNPs (in blue) were only detected on

chromosome 1 (Fvb1) at intervals 7,970,000 to 14,800,000 and 23,450,000 to 23,870,000 bp.

We extended the analysis to small and large insertions/deletions (INDELs) in addition to SNP variants. Within significant intervals, we searched for genes with nonsynonymous variants and ΔSNP-indexes >0.5 and homozygous (SNP-index = to 0 or 1) in the WF pool. The target intervals we identified harbored 105 candidate genes (Supplemental Data Set 1), including FvH4_1g22020 (*FvMYB10*). Bioinformatic analysis of large insertions detected a 52-bp insertion in *FvMYB10* in the WF pool compared to the RF pool and the reference *F. vesca* genome. We focused our analysis on this 52-bp INDEL located at the beginning of the third
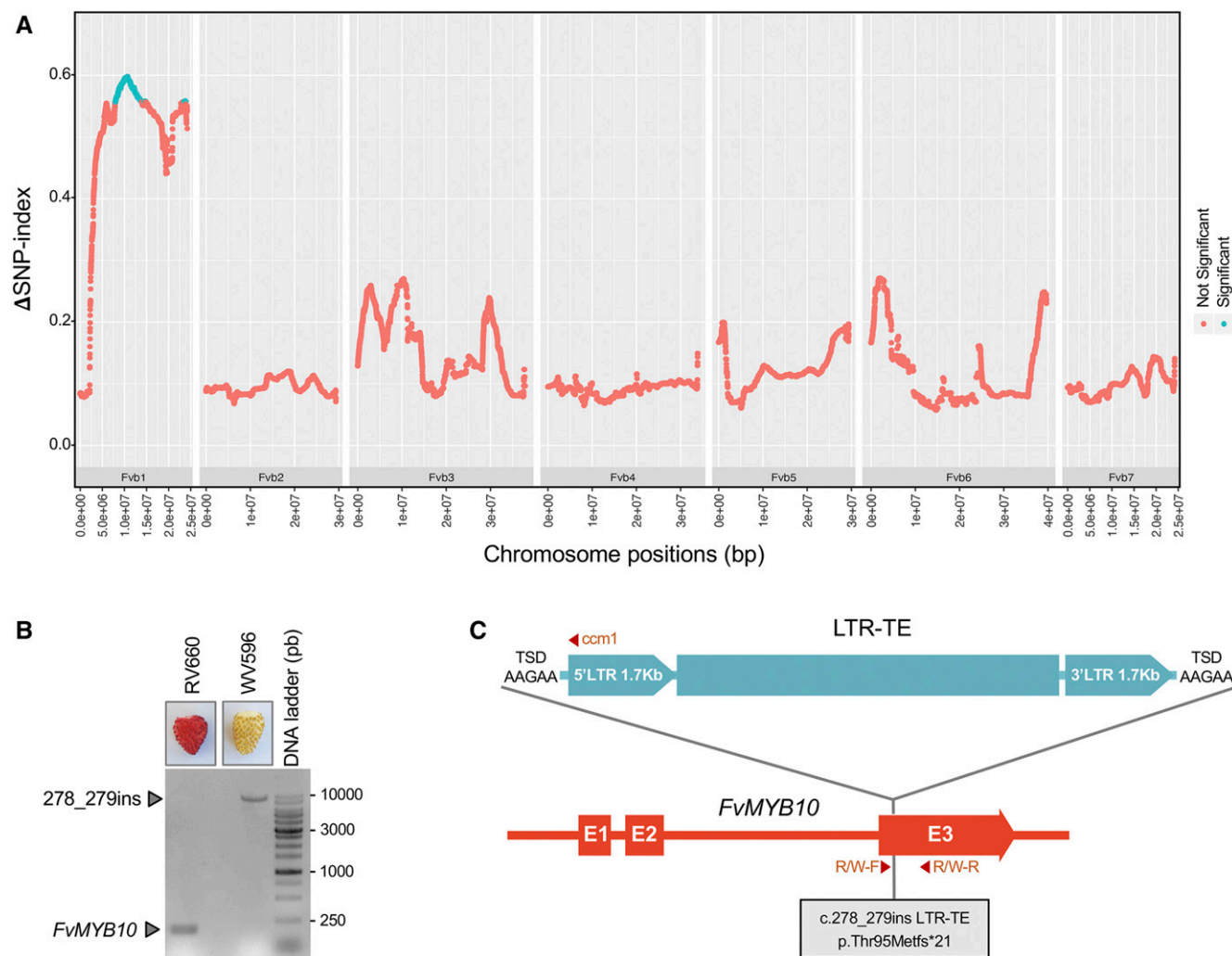
Figure 1. QTL-Seq Identifies a Significant Region on Fvb1 Controlling Fruit Color in RV660 × WV596.

(A) ?SNP-index plot (Y-axis) over the seven *F. vesca* chromosomes. Line represents a sliding window of 3 Mb at 10-kb intervals. Significant SNPs are highlighted in blue (P < 0.03).

(B) *FvMYB10* PCR amplification using primers R/W-F and R/W-R designed flanking the 52 bp INDEL (c.278_279ins). In RV660, the expected fragment size was 181 bp according to the reference Hawaii-4 genome. See scheme in **(C)**.

(C) Schematic representation of FvMYB10-*gypsy*, the Long Terminal Repeat Transposable Element (LTR-TE) identified in the WV596 *FvMYB10* coding sequence. In the scheme, primers used for population genotyping are highlighted (R/W-F, R/W-R, and ccm1, the latter at the 5′ end of the LTR-TE; Supplemental Figure 1).

exon of *FvMYB10*, the strongest candidate mutation underlying the WF phenotype.

The *FvMYB10* Coding Region in White-Fruited WV596 Carries an Long Terminal Repeat-Transposable Element Insertion that Impairs Anthocyanin Accumulation

We designed primers flanking the 52-bp insertion and used them to amplify the corresponding genomic fragment from WF accession WV596 and the RF cv Reine des Vallées (RV660). Standard PCR generated the expected 181-bp product from RV660 but failed to generate a product in WV596. Reanalysis using the long-range 5-Prime PCR Extender System amplified a 10-kb product from WV596 (Figure 1B). Cloning and Sanger sequencing of the 10-kb genomic fragment from WV596 allowed us to confirm the insertion at position 278 of *FvMYB10* cDNA, but it was larger than initially predicted. Further sequencing by primer walking of the entire 10-kb fragment revealed that the insertion located in the third exon of WV596 *FvMYB10* corresponds to a Long Terminal Repeat Transposable Element (LTR-TE), 9509 bp long, belonging to the Gypsy subfamily. This new *FvMYB10* allele was designated *fvmyb10-2,* and the LTR-TE was named FvMYB10-*gypsy.* Upon insertion, FvMYB10-*gypsy* generated the 5 bp AAGAA target site duplication. Two almost identical (one nucleotide substitution) 1.7-kb Long Terminal Repeats (LTRs) were identified flanking the open reading frames (ORFs) necessary for TE replication and transposition (Figure 1C). To determine how tightly linked *fvmyb10-2* was with the WF phenotype in the RV660 × WV596 F_2 population, we used a reverse primer that binds to the FvMYB10-*gypsy* 5′ terminal repeat to genotype the population in combination with primers flanking the insertion point (Figure 1C). The *fvmyb10-2* allele cosegregated with the white phenotype in the entire population (Supplemental Figure 1) following the expected 1:2:1 ratio for a single-gene codominant trait.

FvMYB10 transcript accumulation was not altered in the WF pool upstream of the insertion site but, as expected, it was abolished downstream of the insertion site (Figure 2A). In addition, the LTR-TE sequence introduced a series of premature stop codons in the *FvMYB10* coding sequence. The predicted truncated protein lacks the C-terminal-conserved motif KPRPR[S/T]F for Arabidopsis (*Arabidopsis thaliana*) anthocyanin-promoting MYBs (Stracke et al., 2001); this motif is also found in *Rosaceous MYB10* and known anthocyanin MYB regulators from other species (Lin-Wang et al., 2010). As a result, *fvmyb10-2* is expected to be nonfunctional and unable to induce the expression of FvMYB10 target genes from the anthocyanin pathway. Therefore, we tested the expression of some representative FvMYB10 targets in the *fvmyb10-2* background using RT-qPCR in ripe fruits from the RF and WF pools. As shown in Figure 2A, transcript accumulation from the downstream structural genes *CHI*, *F3H*, *DFR*, *ANS/LDOX*, and *UFGT* was significantly reduced in ripe WF, confirming the notion that *fvmyb10-2* is a loss-of-function allele.

To identify which secondary metabolites were affected by the downregulation of *FvMYB10*, we analyzed ripe fruits in the WF and RF pools by ultra performance liquid chromatography coupled to tandem mass spectrometry (UPLC-Orbitrap-MS/MS). The use of the two bulked pools of F_2 lines instead of parental lines RV660 and WV596 allowed us to identify secondary metabolites affected only

by *FvMYB10* downregulation, excluding the metabolites that differ in the two accessions due to variations in other genes. A total of 88 metabolites were identified, including 30 ellagitannins, 41 flavonoids, 11 hydroxycinnamic acid derivatives, three hydroxybenzoic acid derivatives, and three terpenoids (Supplemental Data Set 2). Significant differences were detected for only 14 metabolites, and the levels of all but one metabolite were increased by FvMYB10 (Figure 2B). As expected, the levels of cyanidin hexose and pelargonidin hexose, the two main anthocyanins, were 625- and 1,950-fold higher in the RF pool, respectively. Mutation of *FvMYB10* reduced the level of one terpenoid (sesquiterpenoid hexose) and one benzoic derivative (hydroxybenzoic acid-hexose) 2.2- and 9-fold, respectively. Interestingly, the mutation in *FvMYB10* reduced the level of ellagic acid hexose 3.4-fold, while that of galloyl-bis (HHDP)-Glc increased 58%. Finally, the levels of one quercetin derivative and six hydroxycinnamic acid derivatives were reduced in the WF pool.

Effects in the same direction on quercetin derivatives and coumaric acid derivatives were observed when *FaMYB10* was transiently downregulated in octoploid strawberry (Medina-Puche et al., 2014) or when *FvMYB10* was engineered in *F. vesca* (Lin-Wang et al., 2014). Other studies that compared secondary metabolites in the fruits of cultivars with different fruit color also demonstrated that quercetin derivatives, coumaric and cinnamic hexoses, and ellagic acid were also associated with MYB10 function (Härtl et al., 2017; Wang et al., 2020). These results indicate that a very limited number of metabolites are affected by MYB10 regulation, suggesting that MYB10 has a primary influence on anthocyanin biosynthesis and effects on a few specific flavonols, ellagitanins, and hydroxycinnamic acids. The reduction in the levels of these metabolites did not affect the total antioxidant capacity of fruits (Supplemental Figure 2). Similarly, no significant differences in total soluble solids content (SSC), titratable acidity, or ascorbic acid content were observed between the RF and WF pools (Supplemental Figure 2). Therefore, fruits that are white due to the downregulation of *MYB10*, like red fruits, are rich sources of nutritional compounds other than anthocyanins.

Finally, we functionally validated *fvmyb10-2* as the causal agent of the lack of anthocyanin accumulation by transiently overexpressing *FvMYB10* in WV596 fruits. Two constructs were generated to test the complementation: $35S_{pro}$:RV660 *FvMYB10* and $35S_{pro}$:WV596 *fvmyb10-2*. RV660 *FvMYB10*, the allele from the RF cv Reine des Vallées, was able to induce anthocyanin accumulation in these fruits, but WV596 *fvmyb10-2* was not (Figure 2C), further confirming the notion that *fvmyb10-2* is the causal gene of the WF phenotype. Previous studies using different *F. vesca* accessions identified an independent polymorphism (G35C) in *FvMYB10* as the underlying cause of anthocyanin-less fruits (Zhang et al., 2015; Hawkins et al., 2016). This specific SNP is translated into a W12S amino acid substitution at a conserved residue within the R2 DNA binding domain and has been identified in five WF *F. vesca* accessions: Hawaii-4, cv Yellow Wonder, cv Pineapple Crush, cv White Soul, and cv White Solemacher. All of these accessions have the C nucleotide and thus the W12S substitution in FvMYB10 (Hawkins et al., 2016). This polymorphism, named *fvmyb10-1* in this study, was not found in WV596, which has the wild-type G nucleotide.
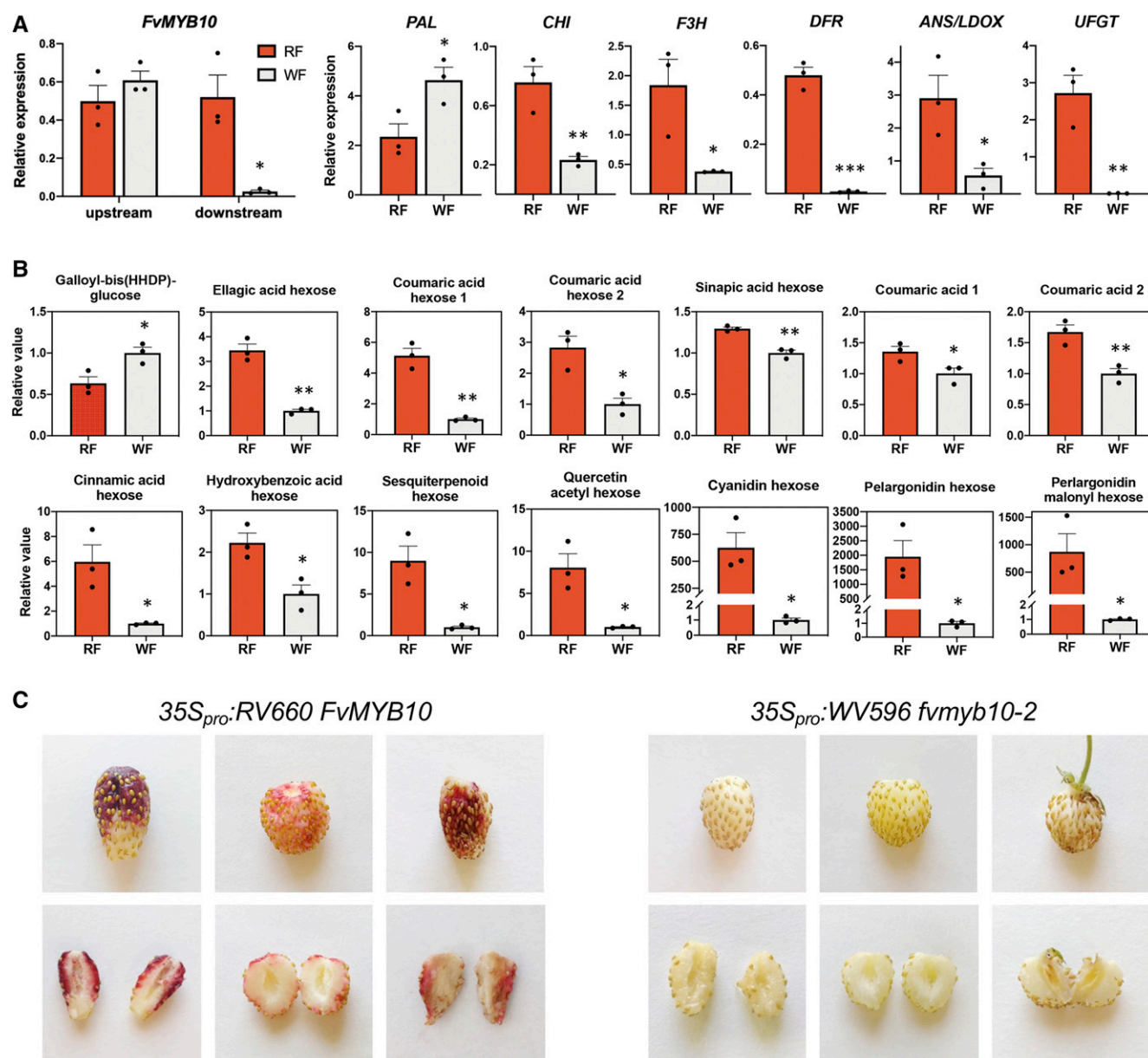
Figure 2. Effect of *FvMYB10* Mutation on Structural Genes and Metabolites in *F. vesca*.

(A) Expression analysis (by quantitative RT-PCR) of *FvMYB10* and anthocyanin structural genes in ripe fruits from RF and WF F_2 pools. For *FvMYB10*, primers were designed upstream (left) and downstream (right) of the LTR-TE insertion point (Supplemental Data Set 11). Means ($\pm$SE) of biological triplicates, consisting of pools of 20 to 25 fruits each, are represented in the graph. Asterisks indicate significant differences, as determined by Student's *t* test (*P < 0.05; ** P < 0.01; *** P < 0.005).

(B) Secondary metabolites with significant differences in levels between RF and WF pools. Means ($\pm$SE) of biological triplicates from RF or WF pools relative to WF pools are represented in the graph. Asterisks indicate significant differences, as determined by Student's *t* test (*P < 0.05; ** P < 0.01).

(C) Transient RV660 *FvMYB10* overexpression restored anthocyanin biosynthesis in WV596 fruits. Three representative fruits are shown. As a control, fruits were agroinfiltrated with the truncated *fvmyb10-2* gene, which failed to induce anthocyanin accumulation.

Independent *FvMYB10* Mutations Explain the Lack of Anthocyanins in Diverse *F. vesca* Ecotypes

To assess the incidence of *fvmyb10-1 or fvmyb10-2* alleles in *F. vesca* accessions with WF color, we broadened our analysis to

include accessions with WFs from different geographic origins: Hawaii-4, cv Yellow Wonder, cv Pineapple Crush, cv White Soul, cv White Solemacher, GER1, GER2, cv South Queensferry, UK13, SE100, and FIN12 (Supplemental Data Set 3). PCR using our newly designed marker revealed that FvMYB10-*gypsy* insertion

(*fvmyb10-2* allele) was not present in any of the accessions analyzed besides WV596 (Figure 3A). In FIN12, we did not detect the FvMYB10-*gypsy* associated band or the endogenous *FvMYB10* gene (Supplemental Figure 3A), pointing to a putative large rearrangement in the surrounding chromosomal region.
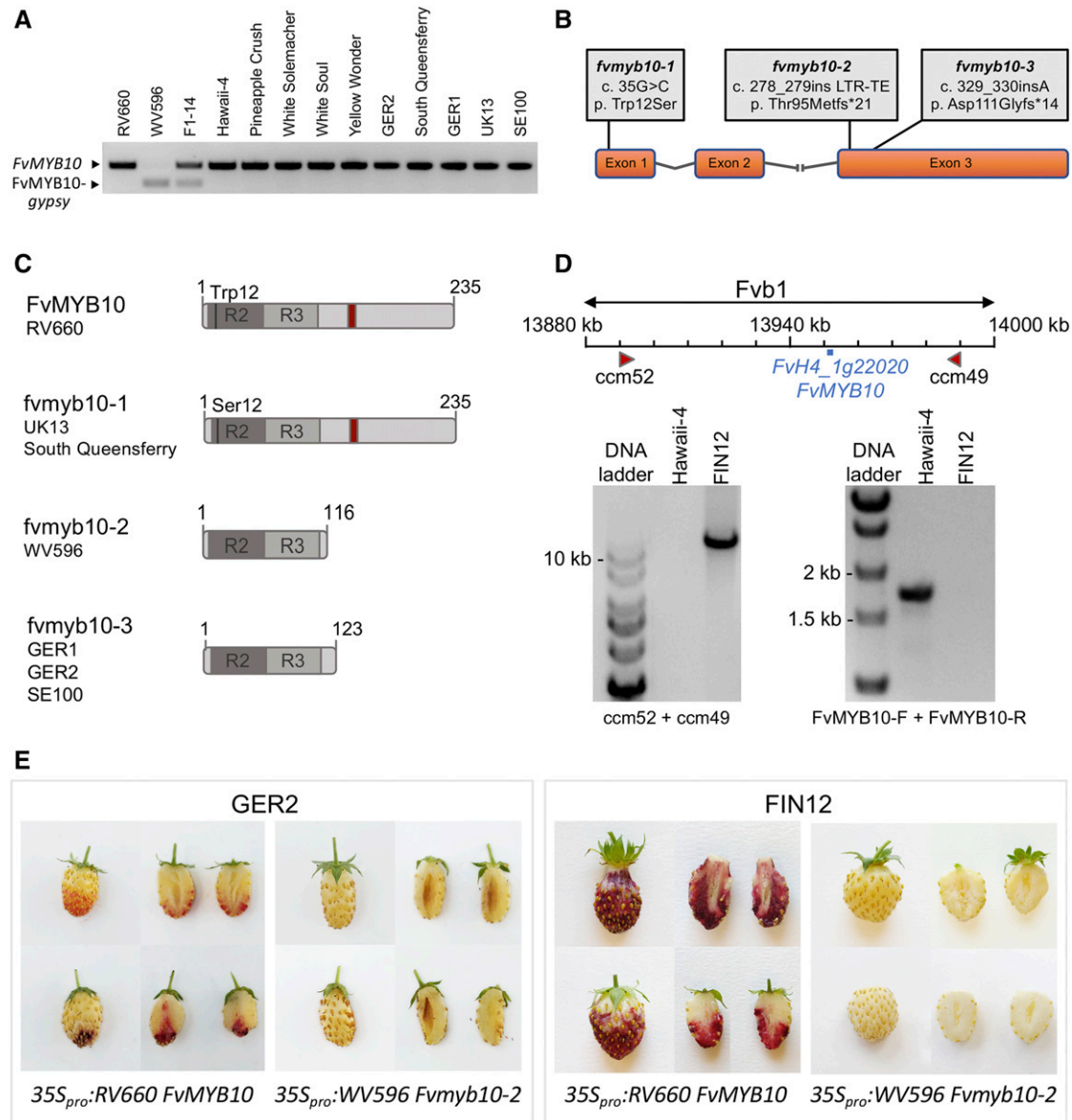
Figure 3. Multiple *FvMYB10* Variants Were Detected in a Panel of 11 White-Fruited *F. vesca* Ecotypes.

(A) FvMYB10-*gypsy* insertion (*fvmyb10-2*) was not detected by PCR analysis in *FvMYB10* from other white-fruited *F. vesca* ecotypes.

(B) Schematic representation of *FvMYB10* showing the three alleles identified in white *F. vesca* ecotypes. *fvmyb10-2* and *fvmyb10-3* were identified in this study, whereas *fvmyb10-1* was previously described by Zhang et al. (2015) and Hawkins et al. (2016).

(C) Outline of the protein products encoded by *FvMYB10* alleles represented in **(B)** and list of the accessions in which they were found. The two repeats (R2R3) of the structurally conserved DNA binding domain are shaded in gray. The conserved motif KPRPR[S/T]F found in anthocyanin MYB regulators is shown in red.

(D) FIN12 has a large deletion in Fvb1 resulting in the loss of 7 predicted genes (Supplemental Figure 3). *FvMYB10* is among them and is highlighted in the scheme. Primers ccm52 and ccm49 were designed flanking the region in Hawaii-4. Both primers are 100 Kb apart, resulting in no PCR product. In FIN12, a >10 kb band was obtained. The picture on the right shows *FvMYB10* CDS amplification with primers FvMYB10-F and FvMYB10-R only in Hawaii-4 but not in FIN12.

(E) *FvMYB10* transient overexpression assays showing complementation of GER2 and FIN12 white fruit. Two representative fruits are shown.

White-fruited ecotypes Hawaii-4, cv Yellow Wonder, cv Pine-apple Crush, cv White Soul, and cv White Solemacher are known to carry the *fvmyb10-1* allele (Hawkins et al., 2016). We cloned the *FvMYB10* CDS from the remaining accessions, GER1, GER2, cv South Queensferry, UK13, SE100, and FIN12, and subjected them to Sanger sequencing. Sequence analysis revealed a third allelic variant previously not described, *fvmyb10-3,* in the accessions from Northern Europe: GER1, GER2, and SE100. The *fvmyb10-3* allele had an A nucleotide insertion at position 329 of the cDNA (c. 329_330insA). The predicted protein contains the Asp111Gly substitution and a frameshift generating a premature stop codon 14 residues downstream from the insertion site (Figures 3B and 3C). Similar to *fvmyb10-2,* the resulting 123 amino acid protein transcribed from *fvmyb10-3* lacks the C-terminal domain found in anthocyanin-related MYB transcription factors (Stracke et al., 2001; Lin-Wang et al., 2010). The British accessions cv South Queensferry and UK13 both carried the previously published *fvmyb10-1* allele with the G35C SNP. In the accession FIN12, we were not able to amplify the *FvMYB10* coding region, but whole genome resequencing of FIN12 revealed an extensive region (~100 kb) in FIN12 chromosome 1 (Fvb1) with extremely low sequence coverage (Supplemental Figure 3B), suggesting that a large deletion affects this chromosomal fragment. The un-covered region of FIN12 roughly corresponds to positions 13,890,000 to 13,990,000 bp from the reference Hawaii-4 ge-nome, which contains seven predicted coding sequences, in-cluding *FvMYB10* (Figure 3D). Primers designed in the predicted flanking regions detected a ~10-kb band in FIN12 but not in Hawaii-4 (Figure 3D), confirming the large deletion from FIN12 Fvb1.

To demonstrate that (1) *fvmyb10-3* in GER1, GER2, and SE100 and (2) the FIN12 large deletion from Fvb1 were the causal mu-tations leading to WFs, we tested whether a functional *FvMYB10* copy was able to restore fruit pigmentation when transiently ex-pressed in fruits from these accessions. The same constructs described for *fvmyb10-2* complementation in WV596 were used in this assay. Once again, the expression of the full-length RV660 *FvMYB10* allele was sufficient to induce anthocyanin accumula-tion in all WF accessions (Figure 3E). Interestingly, anthocyanin accumulation was observed in the fruit epidermis as well as the inner receptacle, where red color is not observed in wild-type fruits. This phenomenon was also observed in WV596 in this study and by Hawkins et al. (2016) when complementing cv Yellow Wonder fruits. This probably resulted from the use of a constitutive 35S promoter, suggesting that *FvMYB10* might not normally be expressed in the internal tissues.

In summary, we identified three *FvMYB10* mutations, in addition to the previously described *fvmyb10-1* allele (Hawkins et al., 2016), which explain the lack of pigmentation in the skin of several white-fruited *F. vesca* accessions: (1) An LTR-TE insertion at the third exon of *FvMYB10* (*fvmyb10-2*); (2) a single nucleotide (A) insertion at position 329 of *FvMYB10* cDNA (*fvmyb10-3)*; and (3) a large deletion in chromosome 1 that removed seven predicted genes, including *FvMYB10*. The different allelic variants affecting fruit color described here are summarized in Supplemental Data Set 3. Notably, none of the WF *F. vesca* accessions we studied carried a functional *FvMYB10* gene. This indicates that the WF phenotype in *F. vesca* arose through different independent mutations in the same *MYB* gene, illustrating a convergent/parallel evolutionary mechanism.

A white-fruited strawberry mutant targeting a gene other than *MYB10* was artificially generated in a previous study. This mutant, the *reduced anthocyanins in petioles* (*rap*) mutant, was identified in a mutagenized *F. vesca* population (Luo et al., 2018). The *RAP* gene encodes a GST that binds anthocyanins to facilitate their transport from the cytosol to the vacuole. Similar WF and white stem phenotypes were observed in cultivated strawberry after *RAP* knockout using clustered regularly interspaced short pal-indromic repeats (CRISPR)/Cas9 (Gao et al., 2020). Neither *rap* mutants nor other mutants in different genes have been identified in nature. We therefore speculate that mutations in genes that result in a general lack of anthocyanins are negatively selected due to the role of anthocyanins in protecting plants against a wide range of abiotic stresses (Tohge et al., 2017), while the lack of anthocyanins only in fruits might not be as detrimental.

Detection of QTLs Controlling Fruit Color in Octoploid Strawberry

The improvement of cultivated strawberry is more challenging than the improvement of the diploid *F. vesca*, not only because of its octoploid genome but also because frequent homoeologous exchanges have occurred following polyploidization, which re-placed substantial portions of some subgenomes with sequences derived from ancestrally related chromosomes (Edger et al., 2019). These exchanges are biased toward the *F. vesca*-like subgenome, although they are not completely unidirectional (Edger et al., 2019). It is therefore crucial to characterize the genetic control of color variation within the octoploid *Fragaria* species and to answer questions such as the following: How many genes are involved in controlling this trait? Are all possible homoeologous copies present in the genome? Are they being expressed? Are previously identified mutations in *FvMYB10* also present in octoploid strawberry?

To accomplish this objective, we studied two diverse octoploid populations characterized by broad variation in fruit skin (Uni-versity of Florida strawberry breeding population 17.66) and flesh color (Hansabred SS×FcL population). The 17.66 population is an F$_1$ derived from biparental cross between two University of Florida (UF) advanced selections (FL 13.65-160 and FL 14.29-1) that segregates for white skin color (Supplemental Figure 4). Within this population, seedlings with white or light pink skin are also char-acterized by white internal flesh. Using the second-generation high-density 50K SNP Array (FanaSNP; Hardigan et al., 2020), we conducted a genome-wide association study (GWAS) to identify the chromosomal regions and specific SNPs associated with skin color in this breeding population. We performed association analyses of 43,422 SNP markers with 95 genotypes to detect marker-trait associations using three different analysis models [a general linear model (GLM), MLM, and multiple-locus mixed model (MLMM)]. SNPs strongly associated with WF skin color were located on chromosome Fvb1-2 (Figure 4A). The most significant SNP marker in all three models was probe AX-184080167, which is adjacent to a *MYB10* homoeolog (Fvb1-2 cv Camarosa, 15,395,876 bp).
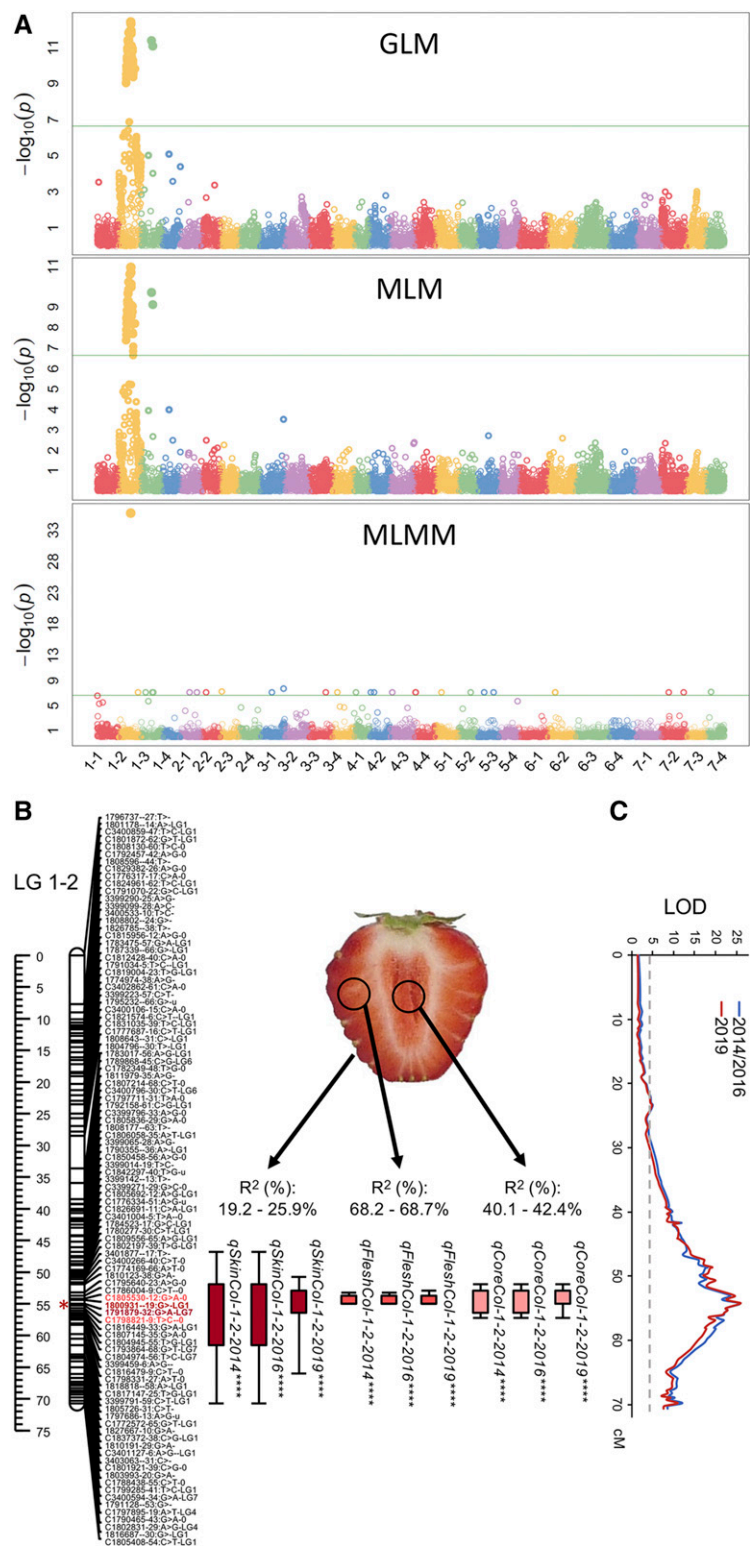
Figure 4. SNPs and QTLs Associated with Fruit Color Traits in Octoploid Strawberry.

(A) Manhattan plots of a GLM, MLM, and MLMM for white fruit in UF breeding population 17.66. Plots for different chromosomes are shown in different colors, which follow the order: chromosome 1-1 to chromosome 7-4. Green line represents the significance threshold.

The second population used in this study, SS×FcL, is an F_2 derived from the interspecific cross between *F.* ×*ananassa* cv Senga Sengana and *F. chiloensis* ssp. *lucida* USA2 that segregates for skin and flesh color in fruits. While all 105 F_2 individuals accumulated various levels of anthocyanins in the skin, the variation in fruit flesh color was somewhat qualitative, with a number of F_2 individuals displaying white flesh (Supplemental Figure 5). The population was phenotyped for skin and flesh color over three seasons and genotyped using DArTseq markers previously developed for octoploid strawberry (Sánchez-Sevilla et al., 2015). Using these data, we generated a linkage map comprising 2991 SNPs and covering a total length of 2377.21 cM (Supplemental Figure 6). Three QTLs (*qSkinCol-1-2*, *qSkinCol-3-1*, and *qSkinCol-2-3*) were detected for fruit skin color. The first QTL was detected in all three years, while the other two were only detected in one or two years (Supplemental Data Set 4). The phenotypic variance contributed by each QTL ranged from 12.2% to 25.9%.

Previous studies have detected QTLs for color traits in LGs belonging to Homoeology group (HG) 1 (Lerceteau-Köhler et al., 2012), 2 (Lerceteau-Köhler et al., 2012; Castro and Lewers, 2016; Zorrilla-Fontanesi et al., 2011), 3 (Lerceteau-Köhler et al., 2012; Zorrilla-Fontanesi et al., 2011), 5 (Zorrilla-Fontanesi et al., 2011; Castro and Lewers, 2016), and 6 (Castro and Lewers, 2016; Lerceteau-Köhler et al., 2012), although the different types of markers used in each study make it difficult to compare LGs and positions. Interestingly, a major QTL for flesh color, *qFleshCol-1-2*, was detected on LG 1-2 in the SS×FcL population in all three years (Figures 4B and 4C). This QTL explained a high proportion of the phenotypic variation (68.2% to 68.7%) and colocalized with *qCoreCol-1-2*, a QTL controlling 40.1% to 42.4% of variation in fruit core color (Figure 4B; Supplemental Data Set 4). The same gene likely affects fruit flesh and core color (internal color), and to a lesser extent skin color, in octoploid strawberry. The 2-logarithm of the odds (LOD) confidence interval of *qFleshCol-1-2* spanned a region on LG 1-2 from 53.2 to 55.0 cM (Supplemental Data Set 4) that corresponds to the region from 13.75 to 15.35 Mb on *F. vesca* chromosome 1 (v4.0.a1; Edger et al., 2018). The 1.6-Mb internal color QTL confidence interval region was found to contain 171 annotated genes. Among these, once again, *MYB10* was the most likely candidate as the gene underlying the QTL.

FaMYB10-2 Is the Dominant Homoeolog in Octoploid Strawberry

As both analysis of UF population 17.66 and SS×FcL studies identified *MYB10* from chromosome Fvb1-2 as a putative causal locus, we further investigated this homoeolog within an octoploid reference genome sequence. The *F.* ×*ananassa* cv Camarosa reference genome (Edger et al., 2019) contains four *FaMYB10*

homoeologs. Chromosomes Fvb1-1 and Fvb1-2 carry one *FaMYB10* homoeolog each: *FaMYB10-1* (maker-Fvb1-1-snap-gene-139.18 or FxaC_4g15020) and *FaMYB10-2* (maker-Fvb1-2-snap-gene-157.15 or FxaC_2g30690), respectively. Two *FaMYB10* genes were found on chromosome Fvb1-3, which were designated *FaMYB10-3A* (maker-Fvb1-3-augustus-gene-143.29 or FxaC_3g25620) and *FaMYB10-3B* (maker-Fvb1-3-augustus-gene-144.30 or FxaC_3g25830), but only *FaMYB10-3B* has a full-length ORF. *FaMYB10-3A* cannot be functional in activating anthocyanin biosynthesis, at least in cv Camarosa, as *MYB10-3A* CDS is interrupted by a Ty1-*copia* retrotransposon insertion at the end of the second intron. As a result, a truncated MYB10 protein lacking the 152 C-terminal residues is predicted. Finally, no *FaMYB10* allele was found on chromosome Fvb1-4.

Therefore, besides *FaMYB10-2*, which is located at the same position as the identified QTL in both octoploid populations, other *MYB10* copies could potentially be functional, as they encode full-length MYB proteins. However, alignment of transcriptomic sequences from a previous RNA-seq study (Sánchez-Sevilla et al., 2017) to the chromosome-scale cv Camarosa genome (Edger et al., 2019) allowed us to obtain subgenome-specific global expression profiles. This subgenome-specific expression analysis revealed that *FaMYB10-2*, in the *F. iinumae*-derived subgenome, is the dominant homoeolog throughout fruit development in strawberry receptacle and achene tissues (Supplemental Figure 7). In pink (turning) and red receptacles, for example, where *FaMYB10* expression peaks, the expression of *FaMYB10-2* represents 97% of total *FaMYB10* expression in the respective ripening stage. By contrast, transcript accumulation from the other two full-length homoeologs from chromosomes Fvb1-1 and Fvb1-3, *MYB10-1* and *MYB10-3B*, was barely detectable, accounting for only 0.6% of total *FaMYB10* expression (Supplemental Figure 7). Similarly, a re-examination of *MYB10* expression from a previous study using 61 strawberry lines (Barbey et al., 2020) demonstrated that *FaMYB10-2* is the dominantly expressed homoeolog compared with those on Fvb1-1 and Fvb1-3. Thus, we expect that a nonfunctional FaMYB10-2 would be sufficient to abolish the induction of the anthocyanin pathway in octoploid strawberry.

Polyploidy, or whole genome duplication, is an important contributor to speciation in flowering plants. The formation of an allopolyploid involves the merger of genomes with separate evolutionary histories and often brings along different mechanisms to compensate for the increased gene dosage, including subgenome dominance. One important factor for subgenome dominance is a lower abundance of methylated TEs relative to other subgenomes (Alger and Edger, 2020). Strawberry is a complex allopolyploid that exhibit dominance in the *F. vesca*-derived subgenome, which contains the lowest TE density (Edger

Figure 4. (continued).

(B) Positions of QTLs on LG 1-2 controlling fruit color detected in the cv Senga Sengana × *F. chiloensis* ssp. *lucida* USA2 F_2 population. Thick and thin bars represent 1- and 2-LOD QTL intervals, respectively, and are drawn to the right of LG 1-2. Names of QTLs as described in Supplemental Data Set 4. Markers in the pick of the QTL and in the 2-LOD interval are highlighted in red and pink, respectively. The estimated position of *FvMYB10* is indicated with an asterisk based on the position of flanking SNPs in *F. vesca* reference genome v.4.

(C) LOD scores of flesh QTL are plotted along the *x* axis (dotted line indicates the 4.5 LOD threshold), while genetic distances are plotted along the *y* axis.

et al., 2019). In particular, chromosomes derived from the *F. vesca* subgenome are responsible for the expression of 88% of structural genes of the anthocyanin biosynthesis pathway (Edger et al., 2019). However, in this study, we demonstrated that anthocyanin biosynthesis is activated predominantly by *MYB10-2,* the homoeolog in the *F. iinumae*-derived subgenome.

MYB10 Allelic Variants in White-Fruited Octoploid Accessions

To identify sequence variation in *MYB10* between white- and red-skinned fruits from UF breeding population 17.66, we performed NGS-based bulked-segregant analysis. *FaMYB10* cDNAs amplified from pools of white- and red-fruited accessions were sequenced using the Illumina MiSeq platform. A total of 242,900 and 236,178 reads were generated in the WF and RF pools, 93.85% and 88.24% of which were mapped in the *FaMYB10-2* gene, respectively. In WF accessions, we found an 8-bp insertion (ACTTATAC) at position 491 of the *FaMYB10-2* ORF generating a premature stop codon and a predicted 179 amino acid protein instead of the 233 amino acid wild-type FaMYB10-2 (Supplemental Figure 8). Deletion of the 54 C-terminal residues may render FaMYB10 inactive. In fact, this same polymorphism was recently shown to be associated with WFs in cv Snow Princess, and the restoration of anthocyanin biosynthesis was only possible when wild-type *MYB10* was overexpressed (Wang et al., 2020). The presence of the same mutation, hereafter named *famyb10-1*, suggests that the white-fruited selection FL 14.29-1 and cv Snow Princess may share a common pedigree.

Unlike in *F. vesca* accessions or in *F.* ×*ananassa* line FL 14.29-1, a comparison of the *MYB10* coding sequence between cv Senga Sengana and USA2, the parents of the SS×FcL F_2 population, revealed no polymorphisms potentially affecting protein stability/functionality. In fact, anthocyanins accumulated in fruit skin in all F_2 individuals, suggesting that a functional *MYB10* gene was expressed in this tissue. To examine the presence of structural variation in the cv Senga Sengana and USA2 *MYB10* promoters (*MYB10_{pro}*), we designed primers based on the Hawaii-4 *F. vesca* reference genome (Shulaev et al., 2011) intended to amplify a ~1-kb product, from −941 to +55 relative to the *FvMYB10* translational start codon (Figure 5A), and used them for PCR in two red- (cv Camarosa and cv Senga Sengana) and three white-fleshed genotypes (USA1, USA2, and FC157). All accessions tested showed the expected ~1-kb amplicon together with an unexpected 1.6-kb band. In accessions with white-fleshed fruits, we detected an extra 2.1-kb band in USA1 and USA2 and a 2.8-kb band in FC157 (Figure 5B). We cloned and sequenced PCR products from cv Senga Sengana, USA2, and FC157, confirming they were all *MYB10_{pro}* alleles.

To assign each *MYB10_{pro}* variant to its respective subgenome, we aligned them with the upstream regulatory sequences of the four cv Camarosa *FaMYB10* homoeologs. Binding sequences of the primers used for *MYB10_{pro}* amplification were localized in all four cv Camarosa homoeologs. The sequence between them was retrieved and used for alignment and homology tree construction together with the different sequenced alleles from cv Senga Sengana, USA2, and FC157 (Figure 5C). The alignment revealed that the region upstream of *MYB10* is extremely polymorphic,

containing a high density of SNPs, INDELs, and transposon-derived sequences. The initially expected ~1-kb product corresponds to the 938 bp long *FaMYB10-3A_{pro}*. All *MYB10-3A_{pro}* alleles from the different backgrounds were grouped in the same clade. All of them were very similar in length (924 to 938 bp) and presented a high degree of sequence conservation (97% to 99% identity). The 1.6-kb allele was common to *MYB10-1* on chromosome Fvb1-1 and *MYB10-3B* on chromosome Fvb1-3. Both *MYB10-1_{pro}* and *MYB10-3B_{pro}* from cv Camarosa were identical and shared 90% identity in the overlapping region with *MYB10-3A_{pro}*. However, *MYB10-3B_{pro}* and *MYB10-1_{pro}* had a 710-bp insertion at position −276 from the initial ATG (green segment in Figure 5C). Interestingly, *MYB10-3A_{pro}* shares higher homology with *F. vesca* *FvMYB10_{pro}* than with *MYB10-3B_{pro}*. This relationship might reflect a chromosome translocation event from Fvb1-4, which did not retain the copy of *MYB10*, rather than a duplication of *MYB10-3B* (or *MYB10-3A*), as according to (Edger et al., 2019), the octoploid chromosome Fvb1-4 originated from the diploid *F. vesca* progenitor. As observed for *MYB10-3A_{pro}*, *MYB10-1_{pro}* and *MYB10-3B_{pro}* alleles from the different accessions were almost identical in length (1641 to 1649 bp) and sequence (96% to 97% identity) and grouped together in the same clade of the homology tree.

Finally, the fourth *FaMYB10_{pro}* allele from the reference cv Camarosa Fvb1-2 chromosome, *FaMYB10-2_{pro}*, turned out to be much longer than the other three homoeologs, that is, almost 23 kb long. This size prevented us from amplifying *FaMYB10-2_{pro}* from cv Senga Sengana and cv Camarosa under routine PCR conditions. Nonetheless, we were able to amplify *MYB10-2_{pro}* alleles from white-fleshed accessions, which were significantly shorter than 23 kb: 2.1 kb in USA1 and USA2, and 2.8 kb in FC157. USA2 *MYB10-2_{pro}* was highly similar to the USA2 *MYB10-1_{pro}* and *MYB10-3B_{pro}* 1.6 kb alleles (94% identity) but it had a tandem duplication of a 471-bp sequence. The first unit of the tandem duplication was a *MYB10-1_{pro}* / *MYB10-3B_{pro}* specific sequence (represented in light green in Figure 5C), and the second unit is colored in blue in the same scheme, highlighting that it is Fvb1-2-specific. On the other hand, FC157 *MYB10-2_{pro}* was almost identical (98% identity) to USA2 *MYB10-2_{pro}*, but FC157 had an additional 660-bp insertion disrupting one unit of the tandem duplicated sequence (dark blue segment in Figure 5C). Despite their tremendous size differences, all *MYB10-2_{pro}* variants were clustered in the same tree branch, as occurred with the other *MYB10_{pro}* homoeologs. Thus, we can conclude that *MYB10_{pro}* alleles from the same homoeolog from different accessions are phylogenetically closer to each other than the four alleles of a given background. Notably, *MYB10-2_{pro}* is the allele that shows higher polymorphism among the different accessions, and the shorter *MYB10-2_{pro}* alleles found in white-fleshed accessions are strong candidates to be the underlying polymorphisms at the *qFleshCol-1-2* QTL and the cause for white flesh in strawberry fruits.

A Large Transposon Insertion in the MYB10-2 Promoter Is Associated with the Red-Flesh Phenotype.

Sequence comparison among the 23-kb cv Camarosa *MYB10-2_{pro}* sequence and the corresponding alleles from the white-fleshed accessions USA2 and FC157 revealed that the
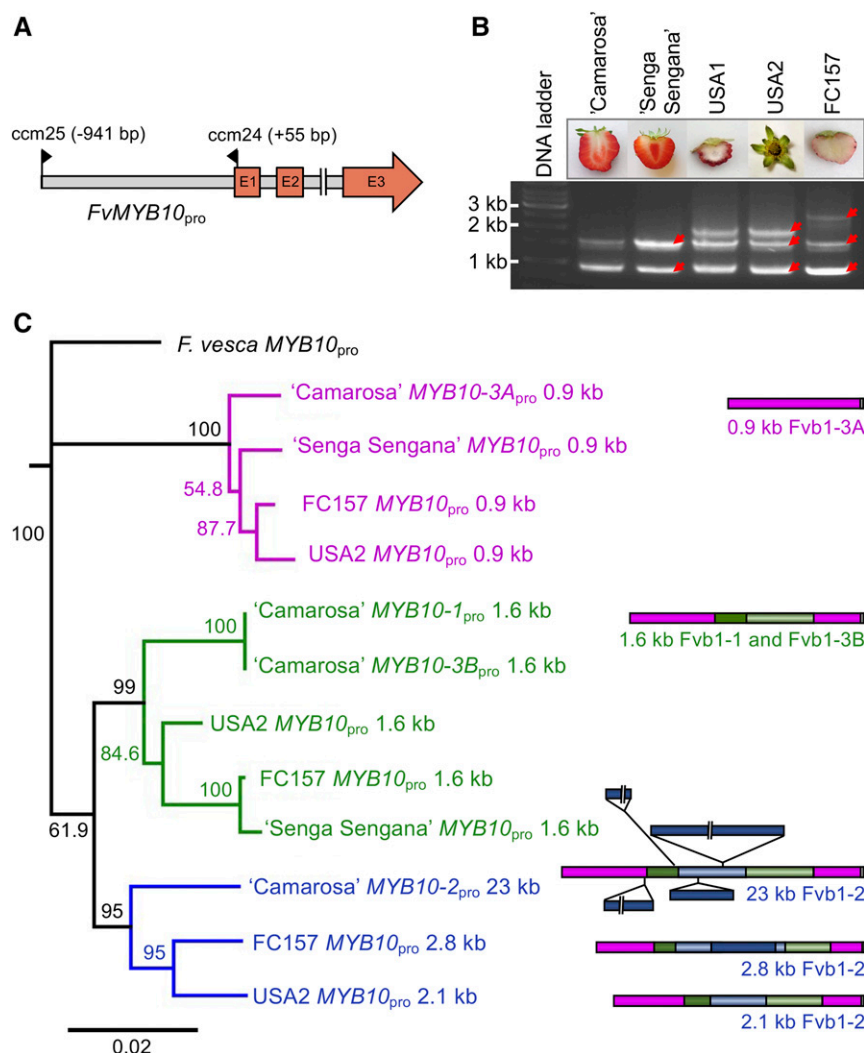
Figure 5. *MYB10* Promoter Variants Across Subgenomes and Accessions in Octoploid *Fragaria* spp.

(A) Schematic representation of *FvMYB10* showing the positions of primers used for PCR amplification of $MYB10_{pro}$ from octoploid *Fragaria* spp (Supplemental Data Set 11).

(B) $MYB10_{pro}$ PCR amplification yielded different sized promoter alleles from each accession. White-fleshed accessions USA1, USA2, and FC157 contained an additional 2.1- or 2.8-kb band compared with red-fleshed ones. Red arrows point to bands that were excised from the gel and cloned for sequencing.

(C) Sequences obtained from **(B)** were aligned with the respective sequences of the four *FaMYB10* homoeologs from cv Camarosa retrieved from the reference genome and analyzed using the Neighbor-Joining method with 1000 bootstrap replicates for homology tree construction. Sequences were grouped in three main clades that revealed their chromosomal origin: (1) Magenta clade contains promoter sequences from all Fvb1-3A homoeologs; (2) green clade from Fvb1-3B and Fvb1-1 homoeologs, which are identical; and (3) in blue, all alleles from Fvb1-2. On the right, a schematic representation of a promoter allele representative of each clade is shown. Three different versions of Fvb1-2 $MYB10_{pro}$ were found: (1) a 23 kb allele from cv Camarosa containing four large INDELs, (2) a 2.1 kb allele from USA2, and (3) a 2.8 kb allele from FC157. A color code was used for each homoeolog copy of $MYB10_{pro}$ in the tree and their respective hallmark sequences in the schemes: Magenta for $MYB10\text{-}3A_{pro}$, green for $MYB10\text{-}1_{pro}$ and $MYB10\text{-}3B_{pro}$ (they are identical), and blue for $MYB10\text{-}2_{pro}$. Bootstrap values >50% are shown in each node. Scale bar indicates substitution rate of nucleotides per site. The branch length is proportional to the nucleotide substitution per site.

common region of cv Camarosa $MYB10\text{-}2_{pro}$ shares 96% identity with alleles from both white-fleshed accessions. The substantial size differences were due to the presence of four large INDELs of 4797, 1496, 454, and 14,064 bp (Figure 5C). These INDELS are located 17.7, 16, 15.4, and 986 upstream of the ATG initiation codon of *MYB10-2,* respectively. With use of the Repbase and the

software tool Censor (Kohany et al., 2006), the 4797- and 14,064-bp insertions were identified as class II (DNA-type) TEs belonging to the CACTA family based on sequence similarity with the *F. vesca EnSpm-1_FV* element (Jurka, 2013; Shulaev et al., 2011). We designated them *FaEnSpm-1* (4797 bp) and *FaEnSpm-2* (14,064 bp). Both elements are bordered by identical 12-bp

terminal inverted repeat sequences 5′-CACTACCAGAAA-3′, and several subterminal direct and inverted repeats were also identified. Upon insertion, *FaEnSpm-1* generated the 3-bp target site duplication TCG, whereas *FaEnSpm-2* is flanked by the target site duplication CAA. *FaEnSpm-2* and *FaEnSpm-1* share important sequence similarity in their internal regions, but *FaEnSpm-1* is thought to be a defective deletion derivative, as most of the sequences have been lost, including two transposase_21 domains (pfam02992; Marchler-Bauer et al., 2015).

The presence of *FaEnSpm-2* at close proximity (<1 kb away) to the *MYB10-2* coding region only in the red-fleshed accessions Camarosa and Senga Sengana prompted us to examine whether its loss correlates with the lack of anthocyanin accumulation in fruit flesh in the SS×FcL mapping population. We developed a co-dominant Fvb1-2-specific PCR marker intended to be predictive for internal fruit color (IFC-1 marker) using a combination of three primers depicted in Figure 6A. When assayed in the entire population, this marked was able to predict the phenotype in >95% of the F$_2$ individuals (Figure 6A). Depending on the season, the phenotypic scores of 4 to 5 out of 105 F$_2$ individuals did not match with their genotypes. This subtle deviation might be explained by the observed variability among fruits from the same line, which could lead to mis-scoring of the phenotype. Alternatively, due to the quantitative nature of this trait, these individuals might represent the natural genetic variation not associated with the large-effect *qFleshCol-1-2* QTL.

The applicability of a given marker in breeding programs depends on its significance beyond a single cross. Therefore, we tested the relevance of our IFC-1 marker and its ability to predict internal fruit color in a wider set of white-fruited *F. chiloensis* accessions. To maximize genetic diversity, we selected accessions from ssp. *chiloensis* (FC156, FC157, FC160, and FC187), ssp. *lucida* (USA1), and ssp. *pacifica* (FC285; Supplemental Data Set 3; Figure 6B). Notably, the 317-bp band associated with the presence of *FaEnSpm-2* was also present in the red-fleshed *F. chiloensis* accession FC154 but was absent from all white-fleshed accessions (Figure 6B). Furthermore, the marker allowed us to identify two different groups of white-fleshed accessions, which also reflect their taxonomic relationships. All *F. chiloensis* ssp. *chiloensis* carried the 2.8-kb *MYB10$_{pro}$* allele (1303 bp band) described for FC157. On the other hand, accessions from ssp. *pacifica* and *lucida*, which are taxonomically closer to each other than to ssp. *chiloensis* (Staudt, 1999), carry the 2.1 kb *MYB10$_{pro}$* allele (645-bp band).

MYB10 and Anthocyanin Biosynthetic Genes Are Upregulated in Red-fleshed Accessions

TEs have the potential to alter or regulate the expression of proximal genes through multiple mechanisms, including the disruption of promoter sequences, introduction of new alternative promoter sequences, and epigenetic silencing (Rebollo et al., 2012; Hirsch and Springer, 2017; Vicient and Casacuberta, 2017). There are multiple examples where the recruitment of a TE in the promoter region of a *MYB10* ortholog leads to its upregulated expression and anthocyanin accumulation in other species such as orange (*Citrus × sinensis*), apple (*Malus × domestica*), pepper (*Capsicum annuum*), and *Brassica oleracea* (Butelli et al., 2012;

Jung et al., 2019; Yan et al., 2019; Zhang et al., 2019). Remarkably, the TE that enhances the expression of the host *MYB* gene in *B. oleracea* and pepper is (like *FaEnSpm-2*) a CACTA element (Jung et al., 2019; Yan et al., 2019). To investigate the association of *FaEnSpm-2* with red flesh color, we performed RNA-seq to profile global gene expression in fruits from cv Senga Sengana and the six white-fleshed accessions previously genotyped in this study except for USA2. USA2 is a male plant and does not set fruits. Instead, we took advantage of its female sister line USA1, which presents the same phenotype segregating in the SS×FcL F$_2$ population (Supplemental Data Set 3). The Fragments per kilobase of transcript per million fragments mapped (FPKM) values for each *MYB10* homoeolog are presented in Figure 6C. As shown for cv Camarosa (Supplemental Figure 7), in cv Senga Sengana, there is an obvious expression level dominance biased toward *MYB10-2*. Interestingly, *MYB10-2* was upregulated in cv Senga Sengana compared to all white-fleshed accessions. Total *MYB10* expression was lower in all white-fleshed accessions too, although transcript accumulation from *MYB10-1* was higher in the four *F. chiloensis* ssp. *chiloensis* accessions compared to cv Senga Sengana, USA1, and FC285, pointing to possible transcriptional compensation.

Comparative analysis of RNA-seq reads from the four *MYB10* homoeologs allowed us to identify SNPs and INDELs among all transcripts relative to the reference cv Camarosa sequence (Supplemental Data Set 5). A total of 15 polymorphic nucleotides were identified in *MYB10* coding regions from the seven samples analyzed. Among these, six were silent mutations, eight were missense mutations at nonconserved residues, and one was a nonsense mutation. None of the previously described polymorphisms in *FvMYB10* or the *FaMYB10* ACTTATAC insertion were present in the analyzed octoploid accessions. The nonsense mutation was only identified in *F. chiloensis* ssp. *chiloensis* accessions (FC156, FC157, FC160, and FC187) and consisted of a G to T transversion at position 478 of *MYB10* ORF. The substitution predicts a premature stop codon at amino acid position 160, generating a truncated protein lacking 74 residues from the C-terminal end (Figure 6D). This new *MYB10* allele derived from *F. chiloensis* was designated *fcmyb10-1*. This allele was found in the three full-length *MYB10* homoeologs from the *F. chiloensis* ssp. *chiloensis* accessions at different allelic dosage (Supplemental Data Set 5). We speculate that the presence of this premature stop codon might be triggering a genetic compensation response (El-Brolosy et al., 2019; Ma et al., 2019) by inducing *MYB10-1* expression (Figure 6C). Remarkably, fruits from three of the *F. chiloensis* ssp. *chiloensis* accessions (FC156, FC160, and FC187) were homozygous for the *fcmyb10-1* allele in Fvb1-2 and are completely white, with no anthocyanins present in the flesh or skin. By contrast, the fourth *F. chiloensis* ssp. *chiloensis* accession, FC157, was heterozygous for the G>T SNP at nucleotide 478 in all *MYB10* homoeologs and has light pink epidermis, indicating once more that the MYB10 C-terminal end is required to induce anthocyanin biosynthesis (Figure 6D). Notably, no color developed in FC157 fruit flesh, suggesting that *MYB10* might not be expressed in this tissue.

We used RNA-seq data to analyze the expression levels of the main structural genes of the anthocyanin biosynthesis pathway, finding that most anthocyanin biosynthesis pathway genes were
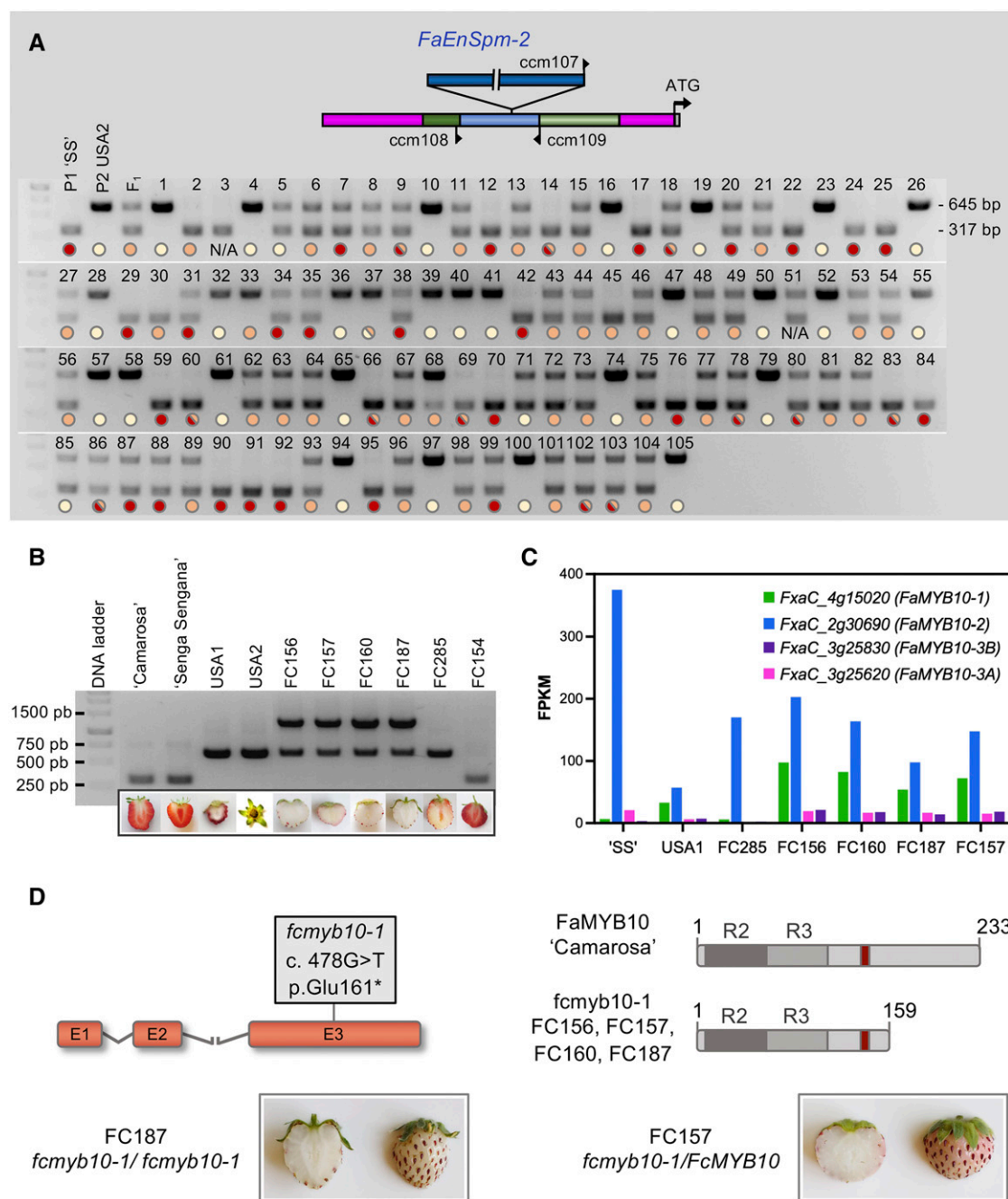
Figure 6. The *FaEnSpm-2* Insertion in the Upstream Regulatory Region of *MYB10-2* Is Associated with Internal RF Color.

Different mutations in the coding sequence lead to completely white fruits lacking anthocyanins in the epidermis.

(A) *FaEnSpm-2* cosegregates with red flesh color in the SS×FcL F$_2$ population. The Fvb1-2-specific codominant IFC-1 marker was developed using a combination of three primers. Primer ccm107 binds to the junction sequence of *FaEnSpm-2* and together with ccm109 amplify a 317-bp band associated with the red-flesh phenotype, whereas the 645 bp product (no TE insertion) associates with the white flesh phenotype. Colored circles indicate flesh color: cream color = 1, orange = 2, and red = 3. Circles with two colors represent different scores from different seasons (Supplemental Figure 5).

(B) IFC-1 marker in *F. chiloensis* accessions. Only the red-fleshed FC154 carried the *FaEnSpm-2* TE at *pMYB10-2*. Among white-fleshed *F. chiloensis*, two different genotypes were found: (1) *F. chiloensis* ssp. *lucida* (USA1 and USA2) and *pacifica* (FC285) accessions both contain the smaller promoter allele version corresponding to the 2.1-kb *pMYB10* variant cloned from USA2, whereas *F. chiloensis* ssp. *chiloensis* accessions (FC156, FC157, FC160, and FC187) harbor the larger 2.8-kb promoter allele identified in FC157.

(C) Data from RNA-seq showing the expression level (FPKM value) of each *MYB10* homoeolog in cv Senga Sengana and six white-fleshed *F. chiloensis* accessions. Expression level dominance is biased toward *MYB10-2* in all accessions tested.

significantly downregulated in all white-fleshed accessions (Figure 7; Supplemental Data Set 6). Transcripts from genes whose products are involved in the early steps of this pathway, including *PAL*, *C4H*, and *4-coumarate:CoA ligase* from the common phenylpropanoid pathway and the early biosynthetic genes *CHS*, *CHI*, and *F3H* were the most strongly affected. However, *UFGT* (a late biosynthetic gene) and *GST* were also notably downregulated in the accessions with the *fcmyb10-1* allele compared to the red-fleshed cv Senga Sengana. *DFR* and *ANS* did not appear to be under the transcriptional control of MYB10: even though they were downregulated in some white-fleshed or completely white accessions, this could be interpreted as a background effect. The most dramatically reduced gene expression levels were found in accessions that were homozygous for the putative nonfunctional *fcmyb10-1* allele on chromosome Fvb1-2: FC156, FC160, and FC187. In these accessions, the expression of *CHS*, *F3H*, *UFGT*, and *GST* was practically abolished, in agreement with the total white phenotype of their fruits, thus confirming that *fcmyb10-1* is a loss-of-function allele.

In USA1 and FC285, the downregulation of some structural genes of the anthocyanin biosynthesis pathway was more moderate, but it should be noted that fruits from these accessions have red epidermis and therefore accumulate anthocyanins. Similar to our results, the downregulation of *FaMYB10* did not affect *ANS* expression in octoploid strawberry (Medina-Puche et al., 2014), while lower *ANS* expression in WFs than RFs was observed in *F. vesca* (Figure 2; Lin-Wang et al., 2014; Härtl et al., 2017). Therefore, FaMYB10 and FvMYB10 may differ in the regulation of *ANS*, as previously suggested (Lin-Wang et al., 2014). Finally, we compared *MYB1* expression levels among the different accessions but found no correlation between fruit color or *MYB10* transcript levels and *MYB1* transcript accumulation (Supplemental Data Set 6), supporting the finding by Medina-Puche et al. (2014) that *FaMYB1* is not under FaMYB10 transcriptional control.

Mining Putative Regulatory Elements in *FaEnSpm-2*

Next, we investigated whether the *FaEnSpm-2* element could be responsible for the activation of *MYB10-2* in red-fleshed fruits by providing novel cis-regulatory sites that behave as enhancers, or that respond to different stimuli and/or provide flesh-specific expression. We used the PlantPAN 3.0 database (Chow et al., 2019) to interrogate the presence of putative transcription factor binding sites (TFBSs) in *MYB10-2* upstream regulatory regions from cv Camarosa and the white-fleshed accessions USA2 and FC157. The cv Camarosa *FaMYB10-2_{pro}* sequence analyzed spanned 3986 bp upstream of the ATG start codon, including the proximal 3 kb of *FaEnSpm-2* element and 986 bp of promoter sequence downstream of the *FaEnSpm-2* insertion site. For USA2

and FC157 *MYB10-2_{pro}* sequences, we surveyed the sequences 2069 and 2729 bp upstream of the initial ATG. All three fragments shared almost 1 kb of the most proximal promoter region downstream of the *FaEnSpm-2* insertion point. In the overlapping region, 36 SNPs and 4 small INDELs were found, not considering the large 660-bp insertion in FC157 *MYB10-2_{pro}*. The results were filtered to a list of 84 putative cis-regulatory elements (at 156 positions) found exclusively at cv Camarosa *FaMYB10-2_{pro}* (Supplemental Data Set 7).

We then focused our analysis on the motifs that are potentially relevant for fruit ripening and anthocyanin biosynthesis. Among these, hormone-responsive elements such as abscisic acid (ABA)- and methyl jasmonate (MeJA)–responsive elements were significantly enriched, with a total of 13 and 4 different putative motifs, respectively (Figure 8A; Supplemental Data Set 8). Additionally, three different MYB binding motifs were identified. These elements might be of special significance, as they could provide a feed-forward mechanism resulting in *MYB10* upregulation. In particular, the BOXLCOREDCPAL (ACCWWCCT) motif, a variant of the conserved MYBPLANT (MACCWAMC) and MYBPZM (CCWACC) elements, is likely to be bound by MYB10, as other R2R3-MYBs involved in phenylpropanoid and anthocyanin biosynthesis bind to this motif (Grotewold et al., 1994; Sablowski et al., 1994; Jian et al., 2019). Notably, the majority of red-flesh associated TFBSs were located within the *FaEnSpm-2* TE, while only 6 elements (at 6 positions) specific to cv Camarosa *FaMYB10-2_{pro}* were detected in the ~1-kb promoter fragment shared by the three accessions (Supplemental Data Set 7).

Cultivated strawberry fruits accumulate anthocyanins in both their flesh and skin, while it is more common to find fruits and vegetables that accumulate anthocyanins only in their skin (Jaakola, 2013; Chaves-Silva et al., 2018). A wide variation in skin and flesh color has also been reported in apple, another *Rosaceae*, and color phenotypes are associated with different alleles of the apple *MYB10* ortholog (Espley et al., 2009; Chagné et al., 2013; Zhang et al., 2019). By contrast, the R1 and R6 motifs found in apple *MYB10* promoters and shown to enhance *MYB10* expression in different species (Espley et al., 2009; Brendolise et al., 2017) were not detected in any of the strawberry promoter sequences analyzed.

Light intensity and quality are important enhancers of anthocyanin biosynthesis, especially in fruit skin (reviewed by Jaakola, 2013). Furthermore, *MYB10* positively regulates light-controlled anthocyanin biosynthesis in apple and strawberry (Lin-Wang et al., 2010; Li et al., 2012; Kadomura-Ishikawa et al., 2015). Independently from light, ABA also promotes *FaMYB10* expression, resulting in the induction of anthocyanin biosynthesis (Medina-Puche et al., 2014; Kadomura-Ishikawa et al., 2015). Strawberry is a nonclimacteric fruit, and ABA plays a crucial role in the ripening process (Chai et al., 2011; Jia et al., 2011). Additionally, Suc can

---

Figure 6. (continued).

(D) Scheme representing the *fcmyb10-1* allele, which contains a G/T SNP in the coding sequence leading to a predicted truncated protein. Accessions homozygous for this variant in Fvb1-2, that is, FC187, are completely white. FC157 is heterozygous *fcmyb10-1/FcMYB10* in chromosome Fvb1-2 (Supplemental Data Set 5) and has a light pink epidermis. The two repeats (R2R3) of the structurally conserved DNA binding domain are shaded in gray. The conserved motif KPRPR[S/T]F found in anthocyanin MYB regulators is shown in red.
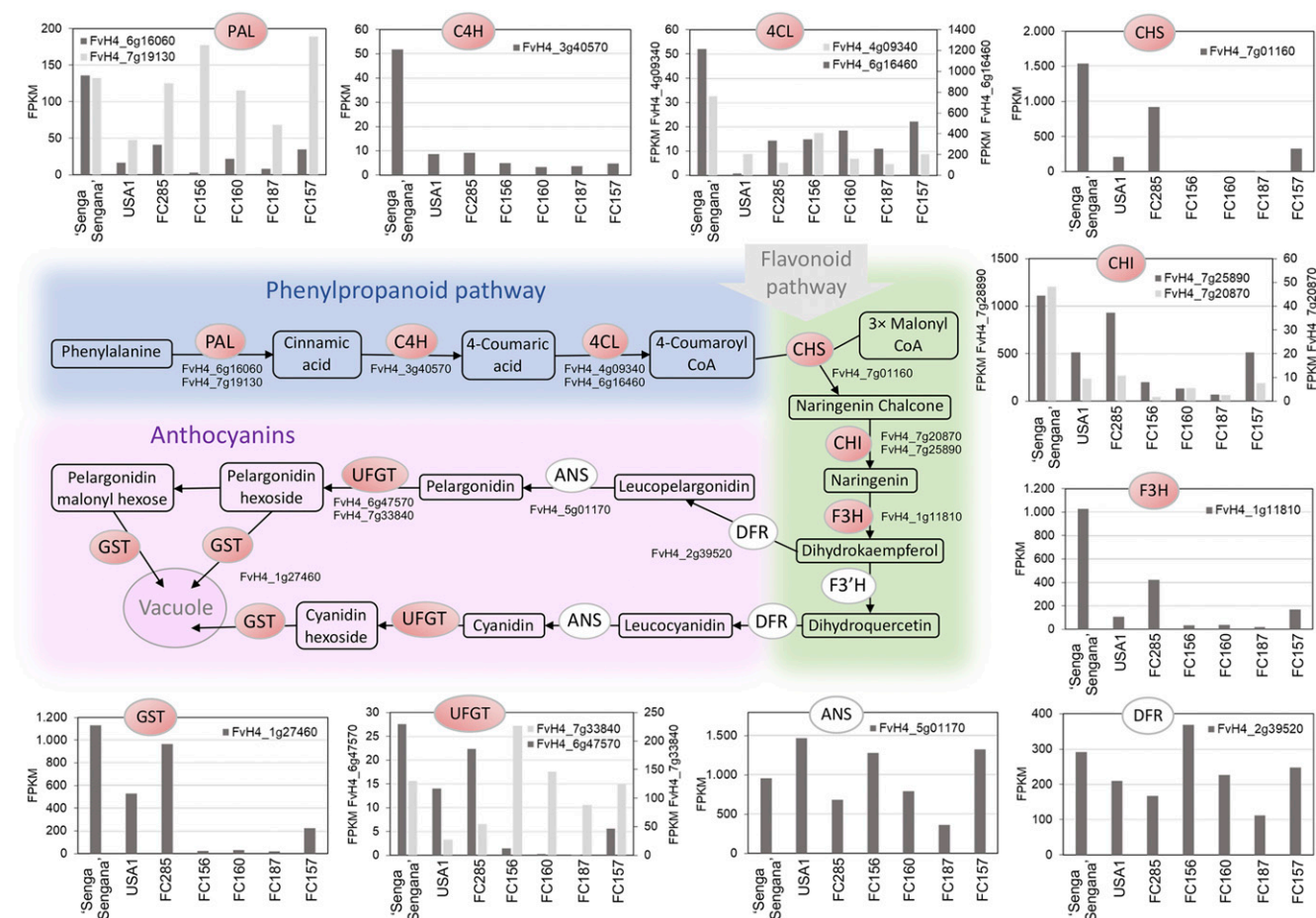
Figure 7. RNA-seq Expression Data of Structural Genes from Anthocyanin Biosynthetic Pathway in cv Senga Sengana and White-Fleshed *F. chiloensis* Accessions.

Mean FPKM values from the biological replicates for each homoeolog of the same gene were added up, and the resulting value represented only if above 10 FPKM. To avoid naming all cv Camarosa homoeologs, each gene was labeled using the corresponding *F. vesca* gene code. Enzymes encoded by genes that are dramatically downregulated in all white-fleshed accessions are highlighted in red. FPKM values and the cv Camarosa gene code for each homoeolog are provided in Supplemental Data Set 6.

induce ABA accumulation and promote strawberry fruit ripening, including anthocyanin accumulation, via ABA-dependent and -independent mechanisms (Jia et al., 2013, 2016; Luo et al. 2019). Finally, MeJA treatment also increases anthocyanin accumulation in strawberry fruit (Concha et al., 2013). Further work will be required to better understand the significance of the predicted putative cis-elements and the molecular mechanisms driving higher *MYB10* expression in red-fleshed accessions. However, it is tempting to speculate that in the interior of the receptacle, where light quality or intensity might not be as effective in inducing *MYB10* expression, other endogenous signals, such as ABA, Suc, or MeJA, would be required to accumulate enough *MYB10* transcript to induce anthocyanin biosynthesis in a light-independent manner. In this scenario, promoters lacking the *FaEnSpm-2* element would not contain the putative regulatory sequences able to recruit the transcription factors that respond to

those stimuli and would fail to induce anthocyanin biosynthesis in the receptacle flesh.

Known *F. vesca* accessions are characterized by red skin and white flesh, while cultivated strawberry cultivars display a characteristic and preferred red interior. Like in the white-fleshed *F. chiloensis* accessions analyzed in this study, *F. vesca* $MYB10_{pro}$ lacks a *FaEnSpm-2-like* TE, as it is not predicted in the *F. vesca* Hawaii4 reference genome (Shulaev et al., 2011) and was not detected by PCR in accessions analyzed in this study such as RV660 or WV596. When putative TFBS were predicted in the homologous $MYB10_{pro}$ region from *F. vesca* (941-bp long), only 5 of the 84 elements exclusively found at cv Camarosa $FaMYB10-2_{pro}$ were detected (Supplemental Data Set 9). None of them were among the selected cis-elements (Supplemental Data Set 8) that are potentially relevant for anthocyanin production in fruit.
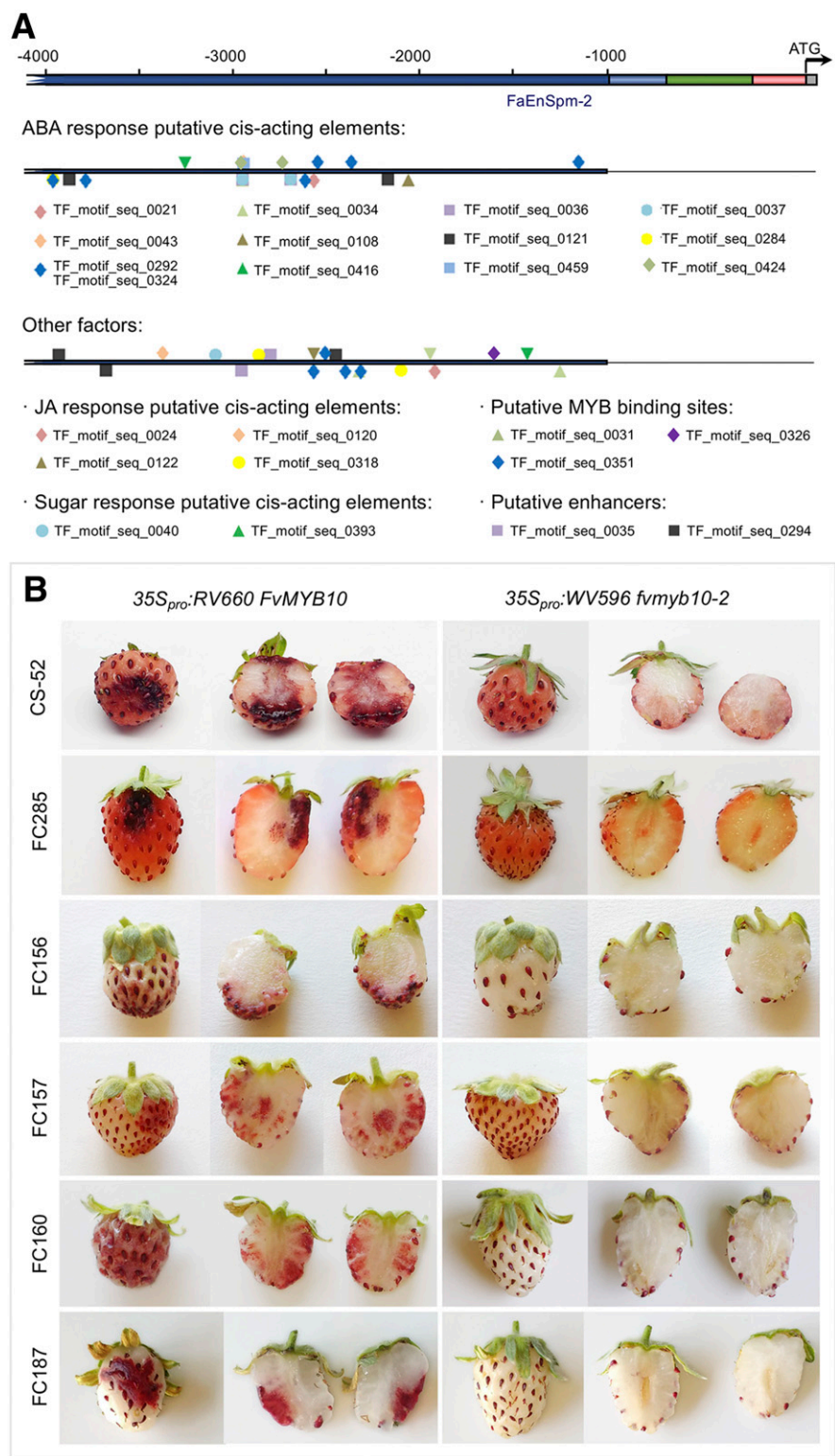
Figure 8. Prediction of Putative Regulatory cis-Elements in the Promoter Region of cv Camarosa *FaMYB10-2* Not Found in *MYB10-2*$_{pro}$ from the White-Fleshed Accessions USA2 or FC157.

Functional validation of *MYB10* as the causal agent under the internal fruit color QTL.

Transient Overexpression of *MYB10* Overcomes White Flesh and Skin Phenotypes in Strawberry Fruit

Finally, if reduced *MYB10* expression in the interior of the receptacle is the underlying cause of white-fleshed phenotype, we reasoned that increasing *MYB10* expression should lead to phenotype complementation. Thus, we performed functional validation in fruits from CS-52, a white-fleshed F_2 line from the SS×FcL population, and the remaining white-fleshed *F. chiloensis* accessions, including FC156, FC157, FC160, FC187, and FC285. In all of these lines, transient expression of RV660 *FvMYB10* under the control of the cauliflower mosaic virus 35S promoter was able to promote anthocyanin accumulation in both fruit flesh and epidermis, but transient expression of the truncated *fvmyb10-2* from WV596 (used as a control) was not (Figure 8B).

Taken together, these results confirm that *MYB10-2*, the *MYB10* homoeolog from the *F. iinumae*-derived subgenome, is the dominant homoeolog in octoploid strawberry and, furthermore, the causal locus responsible for natural variation in internal and external fruit color. Alleles from this locus bearing the *FaEnSpm-2* CACTA element in the upstream regulatory region are associated with enhanced *MYB10* expression, which results in anthocyanin accumulation in the inner receptacle. By contrast, strawberry accessions lacking the TE were characterized by white flesh, while heterozygous lines displayed an intermediate phenotype, indicating incomplete dominance, as also shown by QTL analysis, where the dominance effect of *qFleshCol-1-2* QTL was estimated at 0.24-0.36, depending on the year (Supplemental Data Set 4). We postulate that the increase in *FaMYB10* expression might be due to an expansion of its expression domain into fruit flesh. Additional analysis of *FaEnSpm-2* indicated the presence of putative promoter motifs involved in ABA, MeJA, and sugar responses, as well as predicted MYB binding sites potentially involved in a positive feedback mechanism. Along with the promoter polymorphism, a number of *F. chiloensis* ssp. *chiloensis* accessions with white flesh and skin carry the new *fcmyb10-1* allele at all three full-length homoelogous copies of *FcMYB10*, although at different doses (Supplemental Data Set 5). The predicted fcmyb10-1 is a truncated protein lacking 74 residues from the end portion of the activation domain. We have shown fcmyb10-1 fails to activate the expression of downstream anthocyanin structural genes *PAL, C4H, CHS, F3H,* and *GT*, leading to completely WFs or pink fruits, depending on the allelic dosage (Figure 7). We also found an independent missense mutation, *famyb10-1*, in lines with white skin color from UF breeding population 17.66. This mutation is the same as a previously identified INDEL (Wang et al., 2020). Our study precisely located this mutation to the dominant homoeologous allele on Fvb1-2 and showed that it controls fruit skin color. Whereas polymorphisms found in the coding region appear to be more specific to a subset of accessions, the promoter polymorphism described in this study is common to a taxonomically diverse selection of white-fleshed accessions.

Development of Predictive High-Throughput Markers for Fruit Flesh and Skin Color

The development of high-throughput DNA tests with direct applicability for strawberry breeders has lagged behind that of other crops due to the complexity of the octoploid strawberry genome and the lack of quality subgenome-scale sequence information. Nevertheless, progress in that direction is expected due to the recent release of the first high-quality chromosome-scale octoploid strawberry genome (Edger et al., 2019). Assays for SNP detection such as KASP (Semagn et al., 2013) and high-resolution melting (Wittwer et al., 2003) have become tests of choice for breeders due to their accuracy, ease of scoring, and suitability for polyploid species such as strawberry (Whitaker et al., 2020).

We first developed an HRM marker (WS_CID_01) to predict the presence of the *famyb10-1* allele for the 8-bp INDEL in *MYB10* using the 17.66 population (102 individuals). Marker WS_CID_01 perfectly predicted white and red skin color (Figure 9A; Supplemental Data Set 10). For flesh color prediction, the IFC-1 marker that we developed accurately predicted *MYB10-2* alleles and flesh color phenotypes. However, to develop a more high-throughput assay for marker-assisted selection of white- or red-fleshed strawberries, we designed the KASP marker IFC-2. To identify homoeolog-specific primers that were not expected to amplify *MYB10* homeologs in other subgenomes or other off-target DNA sequences, we aligned the promoter fragments described here to those of cv Camarosa and other octoploid accessions from Hardigan et al. (2020). We identified an A/G SNP 20 bp upstream of the initial ATG and 966 bp downstream of the *FaEnSpm-2* insertion (Supplemental Figure 9). The A allele for the IFC-2 marker was exclusively observed in white-fleshed individuals and accessions. We used the IFC-2 KASP marker to genotype the SS×FcL mapping population ($n = 108$), in addition to two red-fleshed *F. ×ananassa* cvs (Camarosa and Candonga), the red-fleshed *F. chiloensis* accession FC154, and the 6 white-fleshed *F. chiloensis* accessions described earlier. The IFC-2 KASP marker produced codominant genotypic clusters and was 99% predictive of white- and red-fleshed phenotypes (Figure 9B). The red-fleshed allele (G) was observed in the white-fleshed accession FC285, which was the only disparity in our study. The region targeted with this marker is highly polymorphic and even though two common primers accounting for an additional SNP were employed, it might not work in some specific backgrounds. Still, this marker worked in >99% of the genotypes tested, making it a valuable diagnostic tool for breeders. Both the WS_CID_01 and IFC-2 markers should facilitate the rapid introgression of

---

Figure 8. (continued).

(A) Schematic representation of selected regulatory cis-elements exclusively predicted in the cv Camarosa *MYB10-2_pro* allele but not present in the white-fleshed accessions USA2 or FC157. Additional information on these elements can be found in Supplemental Data Set 8.

(B) Complementation of the white flesh phenotype in *F. chiloensis* accessions by transient *FvMYB10* overexpression. A representative fruit from each assay is shown.
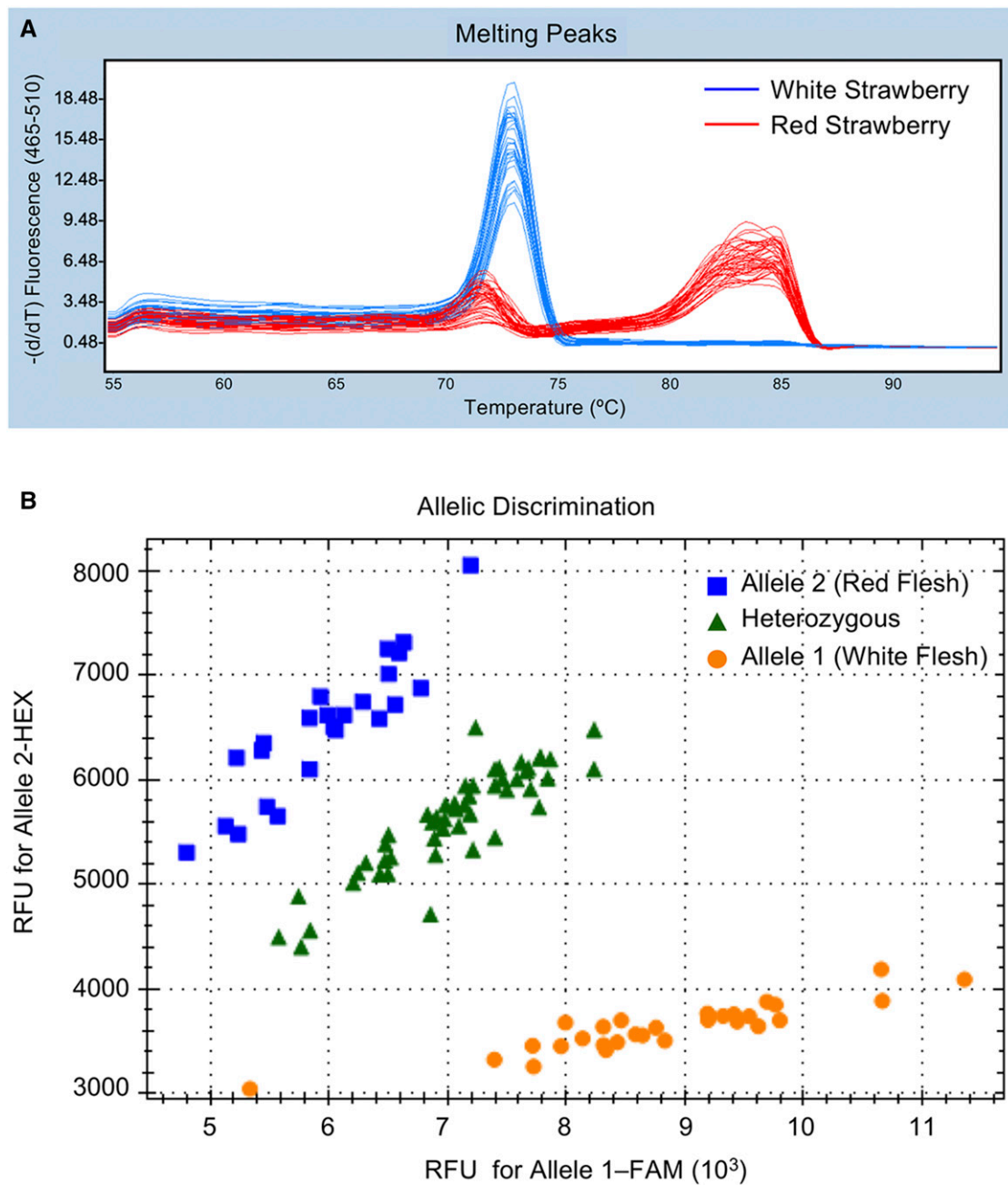
Figure 9. High-throughput Markers for Fruit Skin and Flesh Color.

(A) HRM analysis of the WS_CID_01 marker associated with white fruit color using 102 breeding accessions. The blue and red peaks are associated with white and red color in strawberry, respectively.

(B) Scatterplots of IFC-2 KASP assay results in octoploid strawberry accessions reveal the clustering of white-fleshed lines on the X- (FAM) axis (yellow dots), homozygous red-fleshed lines on the Y- (HEX) axis (blue squares), and heterozygous lines in between (green triangles).

target alleles into elite backgrounds and accelerate the development of white or red-fleshed cultivars, respectively.

Since cultivated strawberry breeding began in the 1800s using a small number of lines (Darrow, 1966), the diversity of F. × ananassa has increased and its genome reshaped by repeated interspecific hybridizations with phylogenetically diverse F.

chiloensis and F. virginiana accessions (Darrow, 1966; Bringhurst and Voth, 1984; Hancock et al., 2001; 2002; Gil-Ariza et al., 2009; Hancock, 1999; Hardigan et al., 2018; Liston et al., 2014). The introgression of beneficial alleles from these species has also resulted in the accumulation of unfavorable alleles in cultivated strawberry. One unwanted trait in most strawberry breeding

programs aimed at developing varieties with red skin is white internal flesh. On the other hand, strawberries with both white skin and white flesh are becoming popular in some countries such as Japan. Furthermore, current breeding programs are particularly directed toward increasing fruit quality and pathogen resistance (Whitaker et al., 2020), and both *F. chiloensis* and *F. virginiana* represent reservoirs of interesting alleles for the future improvement of biotic and abiotic stress tolerance and fruit flavor and aroma (Aharoni et al., 2004; Johnson et al., 2014; Hancock, 1999). Our findings show that *MYB10* exerts simple genetic control over strawberry skin and flesh color, making it a good target for molecular breeding. Therefore, we anticipate that the markers developed in this study will enable efficient advances in breeding, particularly when wild relatives are used as parental lines. Alternatively, CRISPR-Cas9 technology could be used to speed up the breeding process, allowing the direct manipulation of the color trait in any genetic background. CRISPR/Cas9 gene editing has been successfully utilized in both woodland (Zhou et al., 2018) and cultivated strawberries (Martín-Pizarro and Posé, 2018), highlighting the potential of this technique for modifying strawberry fruit color in a more efficient and precise manner.

METHODS

Plant Materials and Phenotypic Evaluation

Diploid *Fragaria vesca* Germplasm

An F_2 mapping population of 145 lines between the everbearing, non-running *Fragaria vesca* cv Reine des Vallées (ESP138.660; RV660) and the WF *F. vesca* ESP138.596 (WV596) was developed from one F_1 plant (F_1-14) that was able to produce runners and had RFs. The population was grown in a greenhouse in Málaga, Spain and phenotyped for two years. The two traits, runnering and red/white fruits, were found to segregate independently as two single mutations. The remaining *F. vesca* accessions were grown under the same conditions and are described in Supplemental Data Set 3 and include cv South Queensferry, GER1, and GER2 from the Günter Staudt collection (Dresden, Germany) and UK13, SE100, and FIN12 from the T. Hytönen and D. Posé collection.

Octoploid *Fragaria* Germplasm

The University of Florida breeding population 17.66 was derived from a cross between FL 13.65-160 (red) and FL 14.29-1 (white) selections (Supplemental Figure 4; Supplemental Data Sets 3 and 8). The population (102 individuals) was grown under open field conditions with two plants per plot. Fruit skin color was assayed three times from December 2018 to February 2019 at the UF/IFAS Gulf Coast Research and Education Center (Balm, Florida).

To generate the SS×FcL F_2 population of 105 progenies, a cross between *Fragaria* ×*ananassa* cv Senga Sengana and *F. chiloensis* ssp. *lucida* USA2 was performed at Hansabred, Germany in 2008 (Supplemental Figure 5). An F_1 seedling, cloned under the number P-90999, was selected among the progeny based on key breeding traits such as tolerance to two spotted spider mite (*Tetranychus urticae* Koch), yield, and fruit aroma and color. The selected F_1 individual was self-pollinated to obtain the F_2 mapping population. The population was grown under field conditions at Hansabred and scored for fruit skin, flesh, and core color in three seasons (2014, 2016, and 2019). Skin color was evaluated using a five-score scale from completely white to dark red. Flesh and core color was evaluated using a three-score scale: 1, white; 2, light red; and 3, red (Supplemental Figure 10). The parental line *F. chiloensis* ssp. *lucida* USA2 is a male

individual that does not set fruit, and therefore USA1, a sister female plant collected from the same area, was included in phenotypic and molecular analyses, as were other *F. chiloensis* accessions from diverse origins (Supplemental Data Set 3).

DNA Extraction and QTL-Seq Analysis of Diploid *Fragaria vesca*

DNA was extracted from young leaves of parental plants, F_1 plants, and each F_2 line using the CTAB method (Doyle and Doyle, 1990) with minor modifications. For rapid mapping of the fruit color mutation, we performed whole-genome resequencing of DNA from two bulked populations as previously described by Takagi et al. (2013). The RF and WF pools were produced by mixing equal amounts of DNA from 34 RF and 32 WF F_2 lines, respectively.

Pair-end sequencing libraries with insert sizes of ~350 bp were prepared, and 100-bp sequences were produced with 50× genome coverage using an Illumina HiSeq 2000. The reads from the RF and WF pools were mapped independently against the latest version of the *Fragaria vesca* reference genome, F_vesca_H4_V4.1 (Edger et al., 2018). The low-quality reads (<Q20 Phred scale) were filtered using the samtools method (Li et al., 2009). Duplicates that originated from PCR were eliminated using the picard-tools program.

For the single nucleotide variants and small INDELs calling process, the gatk algorithm (McKenna et al., 2010) was applied. The large INDELs were identified using the Manta algorithm (Chen et al., 2016). The variants with coverage less than 20 reads in both samples were not considered in downstream analyses.

SNP frequencies in each pool were calculated as the proportion of reads harboring the SNP different from the reference genome. Thus, SNP frequency = 0 if all short reads match the reference sequence and 1 if they correspond to the alternative allele. SNP positions with read depth <7 and frequencies <0.3 in both pools were excluded, as they may represent spurious SNPs called due to sequencing or alignment errors. The parameter ΔSNP-index was calculated as the absolute difference between SNP frequencies in the RF and WF pool samples. To detect significant genomic regions, the genome was split into 3-Mb sliding windows with 10-kb increments. For each window, the average ΔSNP-index was calculated and used for the sliding window plot. To identify statistically significant regions, a Wilcoxon test was applied using a confidence *P*-value of 0.03.

Whole Genome Resequencing of FIN12 and Data Analysis

Whole genome resequencing of the FIN12 accession was performed at DNA Sequencing and Genomics Laboratory, Institute of Biotechnology, University of Helsinki, Finland using an Illumina NextSeq 500 sequencer. Library preparation, pair-end sequencing (150 + 150 bp), and the alignment of the sequencing reads on the *F. vesca* H4 reference genome v4.1 (Edger et al., 2018) were performed as described by Koskela et al. (2017).

GWAS Analysis of F. × *ananassa* Breeding Germplasm

A total of 95 individuals from UF family 17.66 were used for GWAS. Total genomic DNA was isolated from leaf tissues using a modified CTAB method described by Noh et al. (2018). Whole-genome SNP Genotyping was performed using the FanaSNP 50K Array (Hardigan et al., 2020). A GLM, mixed linear model (MLM), and MLMM were used for association tests using GAPIT v2 performed in R (Team, 2014; Liu et al., 2016; Tang et al., 2016). Manhattan plots were created using the R package qqman version 0.1.4 (Turner, 2014).

Linkage Mapping and Detection of QTL in Octoploid *Fragaria*

DNA was extracted from young leaves of parental plants, F_1 plants, and the 105 F_2 lines using the same CTAB method described for diploid *Fragaria*. A

total of 16,070 SNP markers were produced using the strawberry DArTseq platform (Sánchez-Sevilla et al., 2015). SNP markers that were monomorphic in the progeny were removed, and markers that did not fit the expected 3:1 segregation ratio using the χ^2 test (P = 0.05). Next, markers with rowSums <400 were also removed. Finally, markers with more than 5% missing scores (more than five progeny lines) were excluded, resulting in a total of 9005 dominantly scored SNP markers. For 5856 markers, the reference and the alternative allele segregated at a 1:2:1 ratio (as expected for a F_2 population) and were transformed into 2523 codominant markers (COD-SNPs). The 2523 COD-SNPs were used together with 2446 dominant SNPs (DOM-SNPs) for mapping using JoinMap 4.1 (van Ooijen, 2006). First, JoinMap software was used (coding the markers as a CP population) to infer the phases of markers heterozygous in both parental lines and thus of unknown origin in the F_1 line. Phase information was then used to assign phases and to code the SNP markers as a F_2 population. Grouping was performed using independence LOD and the default settings in JoinMap 4.1, and LGs were chosen at a LOD of 9 for all 28 groups obtained. Map construction was performed using the maximum likelihood mapping algorithm and the following parameters: chain length 5,000, initial acceptance probability 0.250, cooling control parameter 0.001, stop after 30,000 chains without improvement, length of burn-in chain 10,000, number of Monte Carlo EM cycles 4, chain length per Monte Carlo EM cycle 2,000, and sampling period for recombination frequency matrix samples 5. A total of 422 identical loci and 517 loci with similarity > 0.99 were removed. The seven HGs were named HG 1 to 7 based on the corresponding LGs in the diploid *Fragaria* reference map. BLAST analysis was performed using the SNP marker sequences as queries against the recently published Camarosa genome and assigned to the best matching chromosome. LGs within homoeologous groups were then named 1 to 4 according to the corresponding Camarosa chromosome number (Edger et al., 2019).

QTL analyses were performed using MapQTL 6 (van Ooijen, 2009). The raw relative data were first analyzed using a nonparametric Kruskal-Wallis rank-sum test. A stringent significance level of P $\leq$ 0.005 was used as a threshold to identify markers linked to QTLs. Second, transformed data sets for nonnormally distributed traits were used to identify and locate mQTLs using Interval Mapping with a step size of 1 cM and a maximum of five neighboring markers. Significance LOD thresholds were estimated with a 1,000-permutation test for each trait. The most significant markers were then used as cofactors for restricted multiple QTL mapping analysis. mQTLs with LOD scores greater than the genome-wide threshold at P $\leq$ 0.05 were declared significant. Linkage maps and QTLs were drawn using MapChart 2.2 (Voorrips, 2002).

RNA Extraction and RT-quantitative PCR

Total RNA was extracted from three independent pools (20 to 25 ripe fruits each) of each WF and RF phenotype. Fruits for these biological triplicates were collected from the same F_2 lines of the 'RV660' × 'WV596' population used for QTL-seq. We followed a CTAB method described by Gambino et al. (2008), with minor modifications. Briefly, 300 mg of powdered fruit sample was used as starting material and RNA was resuspended in 30 μL sterile water. Following digestion with a TURBO DNA-free Kit (Thermo Fisher Scientific AM1907), cDNA was synthesized from 1 μg of RNA using a High-Capacity cDNA Reverse Transcription Kit (Thermo Fisher Scientific 4,368,814). RT-qPCR analysis was performed with iQ SYBR Green Supermix in an iCycler iQ5 system (Bio-Rad) following the manufacturer's instructions. Three technical replicates (within each experiment) were performed for each biological replicate. The relative expression level of a gene of interest in each sample was calculated as $E^{-\Delta Cq}$ and normalized by the $E^{-\Delta Cq}$ value for *GADPH* as the internal reference gene. The sequences of primers used in this study are listed in Supplemental Data Set 11.

Semi-polar Metabolite Analysis Using UPLC-Orbitrap-MS/MS

To investigate the effect of *FvMYB10* mutation, three independent pools of 20 to 25 ripe fruits from each phenotype (RF and WF) were analyzed. Fruits were collected from the same F_2 lines used for QTL-seq and RT-qPCR. Fruit tissue from each pool was ground in liquid nitrogen and stored at −80°C. Secondary metabolite profiles of RF and WF pools were obtained as described by Vallarino et al. (2018) using a Waters Acquity UPLC system. Full documentation of metabolite profiling data acquisition and interpretation is provided in Supplemental Data Set 2.

Quantification of Fruit Quality Parameters

To determine SSC, TA, Trolox equivalent antioxidant capacity (TEAC), and ascorbic acid levels, frozen fruit powder from the same samples (in biological triplicate) used for expression and metabolomic studies were used. For SSC, ~0.5 g of sample was defrosted to room temperature and the puree deposited onto the lens of a refractometer (Atago PR32, Japan). Titratable acidity was evaluated with an automatic titrator (Titroline easy, Schott North America) as previously described by Zorrilla-Fontanesi et al. (2011). Polyphenols were extracted in 80% (v/v) methanol, and the antioxidant capacity of fruit samples was measured based on the ability of antioxidant molecules to quench the ABTS•+ radical cation [2,2′-azino-bis(3-ethylbenzothiazoline-6-sulfonate); Sigma–Aldrich] compared with the antioxidant activity of standard amounts of Trolox. TEAC assays were performed as described (Pellegrini et al., 1999; Re et al., 1999) using 2 μL of sample and 250 μL of radical reagent. The absorbance at 734 nm was measured after 5 min at 25°C in a spectrophotometer. Results were expressed as μmoles of Trolox equivalents per gram of fresh weight (μmol TE/g FW).

L-Ascorbic acid (L-AA) was measured by HPLC (Davey et al., 2006; Zorrilla-Fontanesi et al., 2011). In brief, 0.25 g of fruit powder was homogenized in 1 mL cold extraction buffer (metaphosphoric acid 2% [w/v], EDTA 2 mM) and incubated at 0°C for 20 min. The samples were centrifuged at 14,000 rpm for 20 min at 4°C, and the supernatant was filtered (0.45-mm membrane) and transferred to HPLC vials kept on ice. Finally, a 5-mL sample was injected in a Rx-C18 reverse-phase HPLC column (4.6 × 100 mm, 3.5 mM, Agilent Technologies) and detection was performed at 254 nm in a photodiode array detector (G1315D, Agilent Technologies). The mobile phase consisted of a filtered and degassed solution of 0.1 M NaH_2PO_4, 0.2 mM EDTA pH 3.1 (Harapanhalli et al., 1993), and the flow rate was 0.7 mL/min. L-AA content was calculated by comparison with values obtained from a standard curve and were expressed as mg L-AA per 100 g of fresh weight.

Amplicon Sequence Analysis

Amplicon sequencing was performed using cDNA from WF and RF accessions from UF family 17.66. The fruits from each white-skinned and red-skinned accession were collected in the field, and 2-mm-thick fruit skin samples were collected for RNA extraction using a surgical blade. Total RNA was extracted from each sample with a RNeasy Mini Kit (Qiagen, Germany), and cDNA synthesis was performed using LunaScript RT SuperMix Kit (New England Biolabs, USA) following the manufacturer's instructions. For amplicon sequencing, primer sets were developed for the coding region of *MYB10* (cv Camarosa, maker-Fvb1-2-snap-gene-157.15-mRNA-1) using IDT's PrimerQuest Software (Supplemental Data Set 11). The PCR products were checked in 3% (w/v) agarose gels and further purified for amplicon sequencing at GENEWIZ (South Plainfield, NJ). The sequencing reads from each WF and RF pool (10 samples per pool) were mapped to the *MYB10* gene (maker-Fvb1-2-snap-gene-157.15-mRNA-1) with Geneious v.11.0.5 using default values. The consensus sequences of the *MYB10* coding region of white and red strawberry pools were aligned using T-coffee (Notredame et al., 2000).

Gene and Promoter Cloning and Sequence Homology Analysis

Gene and promoter amplification were performed using MyFi™ DNA Polymerase (Bioline). FvMYB10-*gypsy* and Fvb1 FIN12 genomic fragments flanking the deleted region were amplified with the 5Prime PCR Extender System (5Prime) using the provided 10× Tuning Buffer following the manufacturer instructions.

PCR products <8 kb were purified with a FavorPrep GEL/PCR Purification Kit (Favorgen). PCR products >8 kb were precipitated (30% [w/v] PEG8000; 30mN MgCl₂). Purified products were cloned into the pGEM-T Easy Vector Systems (Promega) for Sanger sequencing.

Multiple sequence alignment of *MYB10* promoter fragments was performed using the Geneious algorithm (Gap open penalty = 30; Gap extension penalty = 0; 50 refinement iterations) and used for homology tree construction (Genetic distance model: Jukes-Cantor; Tree build method: Neighbor-Joining; Resampling method: Bootstrap 1000 replicates), both in Geneious 7.1.9 (Kearse et al., 2012). *F. vesca MYB10$_{pro}$* sequence was chosen as outgroup as it belongs to a different species. Promoter sequence alignment and machine-readable tree files are provided as Supplemental Data Sets 12 and 13.

RNA-Seq Analysis, Differential Gene Expression, and Variant Calling

Total RNA was extracted from two biological replicates of ripe fruits from the seven selected octoploid accessions as described above. Each replicate consisted of a pool of 3 to 5 fruits collected throughout different days at the same time of day (Zeitgeber Time 7). The fruits were immediately frozen in liquid N_2 and stored at −80°C until processing. RNA quantity, quality, and integrity were determined based on absorbance ratios at 260 nm/280 and 260 nm/230 nm using a NanoDrop spectrophotometer (ND-1000 V3.5, NanoDrop Technologies, Inc.) and agarose gel electrophoresis and further verified using a 2100 Bioanalyzer (Agilent, Folsom, CA). Sample RIN values ranged from 7.4 to 8.4. Libraries were produced following Illumina's recommendations at Sistemas Genómicos facilities, where they were sequenced by pair-end sequencing (100 bp × 2) in an Illumina HiSeq 2500 sequencer. Over 200.4 million reads were generated and filtered for high-quality reads by removing reads containing adapters, reads shorter than 50 bp, and reads with Q-value ≤30 using Fastq-mcf from ea-utils (Aronesty, 2011) with the parameters -q 30 -l 50. The following analyses were performed on processed clean reads.

Read mapping, differential gene expression analysis, and clustering of reads from the seven selected octoploid accessions and the previously described cv Camarosa' tissues (Sánchez-Sevilla et al., 2017) were performed using the Tuxedo suit (Hisat2/Cufflinks/CummRbund) following standard procedures (Trapnell et al., 2012). For the reference genome (Edger et al., 2019), we used the latest assembled *F. ×ananassa* genome (Camarosa Genome Assembly v1.0.a1: F_ana_Camarosa_6-28-17.fasta) and annotation (Fxa_v1.2_makerStandard_MakerGenes_woTposases.gff) downloaded from the Genome Database for Rosaceae website (https://www.rosaceae.org/). The overall alignment rate was 90.72%.

Variant calling was performed using the haplotype-based variant detector FreeBayes v1.0.2-16-gd466dde-dirty (Garrison and Marth, 2012). To identify the different variants at each position in the reference *F. ×ananassa* genome, alignment BAM files of the different accessions were labeled with samtools. A VCF file was generated with FreeBayes with all parameters set to default. All bioinformatic processes were performed at the Picasso cluster facilities at Servicio de Supercomputación y Bioinformática Málaga (http://scbi.uma.es).

Transient Overexpression by Agro-infiltration of Fruit

Transient expression studies in strawberry fruits were performed as described (Hoffmann et al., 2006) with minor modifications. Full-length wild-type *FvMYB10* and the truncated *fvmyb10-2* cDNAs were amplified from total cDNA from ripe fruits of the F₂ RV660 × WV596 population RF or WF pools, respectively. Primers FvMYB10-attB1 F and FvMYB10-attB2 R were used to amplify wild-type *FvMYB10*, and FvMYB10-attB1 F and ccm29 were used to amplify *fvmyb10-2* (Supplemental Data Set 11). Primer ccm29 is complementary to a region of the retrotransposon 45 to 70 bp downstream of the insertion point, which includes the first stop codon generated after the insertion. Each gene version was cloned into the Gateway transfer vector pDONR221 and then into the binary vector pK7WG2D under the control of the cauliflower mosaic virus 35S promoter (Gateway BP and LR Clonase II Enzyme mix, Invitrogen). The resulting plasmids were introduced into Agrobacterium strain AGL0 following the protocol of Höfgen and Willmitzer (1988). Immature fruits in the late green/early white stage were used for agro-infiltration using 1 mL suspension of each culture in combination (1:1) with a suspension of Agrobacterium LBA4404 with the p19 suppressor of gene silencing (Voinnet et al., 2003). Agro-infiltrated fruits were labeled and left to ripen in planta for ~7 to 10 d.

HRM Marker Development and Marker Data Analysis

The primer set targeting the 8-bp mutation was designed using IDT's PrimerQuest Software and ordered from IDT (San Jose, California; Supplemental Data Set 11). PCR amplification was performed in a 5 μL reaction containing 0.5 μM of each primer set, 2× AccuStart™ II PCR ToughMix (Quantabio, Beverly, Massachusetts), 1× LC Green Plus HRM dye (BioFire, Salt Lake City, Utah), and 0.5 μL of DNA. The PCR conditions were as follows: an initial denaturation at 95°C for 5 min; 45 cycles of denaturation at 95°C for 10 s, annealing at 62°C for 10 s, and extension at 72°C for 20 s. After PCR amplification, the samples were heated to 95°C for 1 min and cooled to 40°C for 1 min. Melting curves were obtained by melting over the desired range (60° to 95°C) at a rate of 50 acquisitions per 1°C. The HRM assay was performed with the LightCycler 480 System II (Roche Life Science, Germany). The HRM data were analyzed using Melt Curve Genotyping and Gene Scanning Software (Roche Life Science, Germany). Analysis of HRM variants was based on differences in the shapes of the melting curves and Tm values.

SNP Genotyping using KASP

An SNP in *MYB10-2* at position −20 from the initial ATG associated with white/red flesh color in the sequenced accessions was targeted for the KASP assay. To produce a subgenome-specific assay, a combination of four primers was used in each reaction: two common forward primers (ccm90 and ccm91) to account for a background-specific G/A SNP, and two allele-specific primers (ccm92 and ccm93), each carrying the standard FAM or HEX dye tails and the targeted SNP at the 3′ end. A single common primer is generally used for standard KASP assays, but the high degree of polymorphism in the targeted region made it necessary to include an extra common forward primer to account for a different, background-associated G/A SNP not linked to the white-fleshed trait. Reaction volumes of 5 μL for 384-well plates were used; 2.5 μL of MasterMix, 0.07 μL of assay/primer mix, and 2.5 μL of DNA (12.5 ng total) were used for genotyping. The final primer concentrations in the reaction mix were 210 nM for ccm90 and ccm91; 150 nM for ccm92; and 190 nM for ccm93. PCR was conducted in a BioRad CFX-384 instrument using the following protocol: An initial denaturation step at 94°C for 15 min, 12 touchdown cycles (94°C for 20 s, 65°C for 80 s, dropping 0.6°C per cycle), 29 cycles (94°C for 20 s, 58°C for 80 s), and a final recycling for 2 cycles (94°C for 20 s, 60°C for 80 s). BioRad software was used to estimate the final results.

Accession Numbers

F. vesca FIN12 accession sequencing data are stored at National Center for Biotechnology Information Short Read Archive (https://www.ncbi.nlm.nih.gov/sra) under accession number PRJNA655237.

The raw reads data from (1) Illumina high-throughput sequencing of RF and WF DNA pools from F_2 lines of the *F. vesca* RV660 × WV596 population and (2) RNA-seq from ripe fruits of white and red octoploid accessions were stored at the Sequence Read Archive (SRA) of the European Nucleotide Archive (ENA) under project reference number PRJEB38128. In the same project, Sanger sequences were stored under the following specific codes: (1) *fvmyb10-3* mutant alleles sequences from SE100, GER1, and GER2: LR862245, LR862246, and LR862247; (2) *MYB10* promoter sequences from *F. chiloensis* ssp. *chiloensis* FC157 *MYB10-1$_{pro}$/MYB10-3B$_{pro}$*, *MYB10-2$_{pro}$*, and *MYB10-3A$_{pro}$* (LR862237-LR862239), *F. chiloensis* ssp. *lucida* USA2 *MYB10-3A$_{pro}$*, *MYB10-1$_{pro}$/MYB10-3B$_{pro}$*, and *MYB10-2$_{pro}$* (LR862240-LR862242), *Fragaria* × *ananassa* cv Senga Sengana *MYB10-3A$_{pro}$* and *MYB10-1$_{pro}$/MYB10-3B$_{pro}$* (LR862243- LR862244); and (3) The FvMYB10-*gypsy* LTR-TE sequence from *fvmyb10-2*: LR8622681.

Supplemental Data

Supplemental Figure 1.. The LTR-TE insertion in *FvMYB10* cosegregates with the white fruit phenotype in the entire RV660xWF596 population.

Supplemental Figure 2.. TEAC, soluble solid content (SSC), titratable acidity (TA), and L-ascorbic acid (L-AA) content in RF and WF F2 pools of the RV660 x WV596 population.

Supplemental Figure 3.. *F. vesca accession* FIN12 has a large deletion affecting an ~100 kb region in Fvb1 that results in the loss of seven predicted genes including *FvMYB10* (*FvH4_1g22020*).

Supplemental Figure 4.. Fruit skin color in UF population 17.66 (FL 13.65-160 × FL 14.29-1).

Supplemental Figure 5.. Fruit flesh and skin color phenotypes in the Hansabred SS×FcL population.

Supplemental Figure 6.. Senga Sengana x *F. chiloensis* ssp. *lucida* linkage map and comparison to the physical positions in the *F. vesca* reference genome.

Supplemental Figure 7.. Expression of cv Camarosa *FaMYB10* homoeologs in different tissues and during fruit ripening.

Supplemental Figure 8.. Sequence alignment of WT and mutant MYB10-2 in UF breeding population 17.66.

Supplemental Figure 9.. Alignment of the *MYB10* upstream region showing the SNP targeted for KASP genotyping.

Supplemental Figure 10.. Fruit color scale used to phenotype octoploid accessions.

Supplemental Data Set 1.. List of significant SNPs and INDELs in the RV660 × WV596 population.

Supplemental Data Set 2.. Complete metabolite data.

Supplemental Data Set 3.. List of *Fragaria* ssp. included in this study and description of mutations detected in *MYB10*.

Supplemental Data Set 4.. QTLs detected for fruit color traits in the cv Senga Sengana × *Fragaria chiloensis* ssp. *lucida* F_2 population by Kruskal-Wallis (KW) and restricted multiple QTL mapping (rMQM) analysis.

Supplemental Data Set 5.. Polymorphisms at *MYB10* homoeologs from *F. chiloensis* accessions and cv Senga Sengana *vs.* the cv Camarosa reference genome.

Supplemental Data Set 6.. Expression of anthocyanin pathway genes in cv Senga Sengana and white-fleshed *F. chiloensis* accessions.

Supplemental Data Set 7.. Predicted putative cis-elements specific to cv Camarosa *FaMYB10-2$_{pro}$*.

Supplemental Data Set 8.. Predicted putative cis-elements specific to cv Camarosa *FaMYB10-2$_{pro}$* potentially significant in the context of fruit ripening and anthocyanin production.

Supplemental Data Set 9.. Putative cis-elements predicted in *FvMYB10$_{pro}$* overlapping with those exclusively predicted in cv Camarosa *FaMYB10-2$_{pro}$*.

Supplemental Data Set 10.. Phenotypes and WS_CID_1 marker genotypes of UF breeding population 17.66 (FL 13.65-160 × FL 14.29-1).

Supplemental Data Set 11.. List of primers.

Supplemental Data Set 12.. Sequence alignment file in fasta format of *MYB10$_{pro}$* variants.

Supplemental Data Set 13.. Machine-readable tree file of *MYB10$_{pro}$* variants.

AUTHOR CONTRIBUTIONS

C.C. and I.A. planned and designed the experiments, analyzed the data, and wrote the article with input from all other authors.; C.C., performed molecular analyses, phylogenies, expression analysis by RT-qPCR, and transient overexpression by agro-infiltration of fruits; V.W, H.W., and K.O. developed the octoploid SS×FcL mapping population and performed the phenotypic analysis; R.R. and I.A. performed the genetic mapping and QTL analysis in the octoploid SS×FcL population; N.O. and P.M. performed fruit quality assessments; J.C.T, J.C., Z.L., and I.A. performed the genetic mapping in diploid *F. vesca*; N.C., M.A.H., and S.J.K. provided genomic data for the cultivated and wild octoploid accessions and participated in KASP marker development; J.G.V. and S.O. conducted the metabolomics analysis; C.M.-P., D.P., T.T., and T.H. provided genomic data for the wild *F. vesca* accessions; Y.O., C.R.B., and V.M.W. developed the 17.66 population and assisted Y.O. and S.L. in phenotyping. S.L. performed genetic and molecular analyses of UF family 17.66; J.F.S.-S. performed RNA-seq and bioinformatic analyses of octoploid strawberry.

REFERENCES

Aharoni, A., De Vos, C.H., Wein, M., Sun, Z., Greco, R., Kroon, A., Mol, J.N., and O'Connell, A.P. (2001). The strawberry *FaMYB1* transcription factor suppresses anthocyanin and flavonol accumulation in transgenic tobacco. Plant J. **28:** 319–332.

Aharoni, A., Giri, A.P., Verstappen, F.W.A., Bertea, C.M., Sevenier, R., Sun, Z., Jongsma, M.A., Schwab, W., and Bouwmeester, H.J. (2004). Gain and loss of fruit flavor compounds produced by wild and cultivated strawberry species. Plant Cell **16:** 3110–3131.

Alger, E.I., and Edger, P.P. (2020). One subgenome to rule them all: Underlying mechanisms of subgenome dominance. Curr. Opin. Plant Biol. **54:** 108–113.

Allan, A.C., Hellens, R.P., and Laing, W.A. (2008). MYB transcription factors that colour our fruit. Trends Plant Sci. **13:** 99–102.

Almeida, J.R.M., D'Amico, E., Preuss, A., Carbone, F., de Vos, C.H.R., Deiml, B., Mourgues, F., Perrotta, G., Fischer, T.C., Bovy, A.G., Martens, S., and Rosati, C. (2007). Characterization of major enzymes and genes involved in flavonoid and proanthocyanidin biosynthesis during fruit development in strawberry (Fragaria xananassa). Arch. Biochem. Biophys. **465:** 61–71.

Aronesty, E. (2011). ea-utils: "Command-line tools for processing biological sequencing data"; https://github.com/ExpressionAnalysis/ea-utils.

Barbey, C., Hogshead, M., Schwartz, A.E., Mourad, N., Verma, S., Lee, S., Whitaker, V.M., and Folta, K.M. (2020). The genetics of differential gene expression related to fruit traits in strawberry (Fragaria ×ananassa). Front Genet. **10:** 1317.

Brendolise, C., Espley, R.V., Lin-Wang, K., Laing, W., Peng, Y., McGhie, T., Dejnoprat, S., Tomes, S., Hellens, R.P., and Allan, A.C. (2017). Multiple copies of a simple MYB-binding site confers trans-regulation by specific flavonoid-related R2R3 MYBs in diverse species. Front Plant Sci **8:** 1864.

Bringhurst, R.S., and Voth, V. (1984). Breeding octoploid strawberries. Iowa State J. Res. **58:** 371–381.

Brown, T., and Wareing, P.F. (1965). The genetical control of the everbearing habit and three other characters in varieties of Fragaria vesca. Euphytica **14:** 97–112.

Butelli, E., Licciardello, C., Zhang, Y., Liu, J., Mackay, S., Bailey, P., Reforgiato-Recupero, G., and Martin, C. (2012). Retrotransposons control fruit-specific, cold-dependent accumulation of anthocyanins in blood oranges. Plant Cell **24:** 1242–1255.

Carbone, F., Preuss, A., De Vos, R.C.H., D'Amico, E., Perrotta, G., Bovy, A.G., Martens, S., and Rosati, C. (2009). Developmental, genetic and environmental factors affect the expression of flavonoid genes, enzymes and metabolites in strawberry fruits. Plant Cell Environ. **32:** 1117–1131.

Castro, P., and Lewers, K.S. (2016). Identification of quantitative trait loci (QTL) for fruit-quality traits and number of weeks of flowering in the cultivated strawberry. Mol. Breed. **36:** 138.

Chagné, D., et al. (2013). An ancient duplication of apple MYB transcription factors is responsible for novel red fruit-flesh phenotypes. Plant Physiol. **161:** 225–239.

Chai, Y.M., Jia, H.F., Li, C.L., Dong, Q.H., and Shen, Y.Y. (2011). FaPYR1 is involved in strawberry fruit ripening. J Exp Bot **62:** 5079–5089.

Chaves-Silva, S., Santos, A.L.D., Chalfun-Júnior, A., Zhao, J., Peres, L.E.P., and Benedito, V.A. (2018). Understanding the genetic regulation of anthocyanin biosynthesis in plants - Tools for breeding purple varieties of fruits and vegetables. Phytochemistry **153:** 11–27.

Chen, X., Schulz-Trieglaff, O., Shaw, R., Barnes, B., Schlesinger, F., Källberg, M., Cox, A.J., Kruglyak, S., and Saunders, C.T. (2016). Manta: Rapid detection of structural variants and indels for germline and cancer sequencing applications. Bioinformatics **32:** 1220–1222.

Chow, C.-N., Lee, T.-Y., Hung, Y.-C., Li, G.-Z., Tseng, K.-C., Liu, Y.-H., Kuo, P.-L., Zheng, H.-Q., and Chang, W.-C. (2019). PlantPAN3.0: A new and updated resource for reconstructing transcriptional regulatory networks from ChIP-seq experiments in plants. Nucleic Acids Res. **47** (D1): D1155–D1163.

Concha, C.M., Figueroa, N.E., Poblete, L.A., Oñate, F.A., Schwab, W., and Figueroa, C.R. (2013). Methyl jasmonate treatment induces changes in fruit ripening by modifying the expression of several ripening genes in Fragaria chiloensis fruit. Plant Physiol. Biochem. **70:** 433–444.

Darrow, G.M. (1966). The strawberry. History, breeding and physiology. (New York: Holt, Winston, Rinehart).

Davey, M.W., Kenis, K., and Keulemans, J. (2006). Genetic control of fruit vitamin C contents. Plant Physiol. **142:** 343–351.

Del Rio, D., Rodriguez-Mateos, A., Spencer, J.P.E., Tognolini, M., Borges, G., and Crozier, A. (2013). Dietary (poly)phenolics in human health: Structures, bioavailability, and evidence of protective effects against chronic diseases. Antioxid. Redox Signal. **18:** 1818–1892.

Deng, C., and Davis, T. (2001). Molecular identification of the yellow fruit color (c) locus in diploid strawberry: A candidate gene approach. Theor. Appl. Genet. **103:** 316–322.

Doyle, J.J., and Doyle, J.L. (1990). Isolation of plant DNA from fresh tissue. Focus **12:** 13–15.

Duan, W., Sun, P., and Li, J. (2017). Expression of genes involved in the anthocyanin biosynthesis pathway in white and red fruits of Fragaria pentaphylla and genetic variation in the dihydroflavonol-4-reductase gene. Biochem. Syst. Ecol. **72:** 40–46.

Edger, P.P., et al. (2019). Origin and evolution of the octoploid strawberry genome. Nat. Genet. **51:** 541–547.

Edger, P.P., et al. (2018). Single-molecule sequencing and optical mapping yields an improved genome of woodland strawberry (Fragaria vesca) with chromosome-scale contiguity. Gigascience **7:** 1–7.

Edger, P.P., McKain, M.R., Yocca, A.E., Knapp, S.J., Qiao, Q., and Zhang, T. (2020). Reply to: Revisiting the origin of octoploid strawberry. Nat. Genet. **52:** 5–7.

El-Brolosy, M.A., et al. (2019). Genetic compensation triggered by mutant mRNA degradation. Nature **568:** 193–197.

Espley, R.V., Brendolise, C., Chagné, D., Kutty-Amma, S., Green, S., Volz, R., Putterill, J., Schouten, H.J., Gardiner, S.E., Hellens, R.P., and Allan, A.C. (2009). Multiple repeats of a promoter segment causes transcription factor autoregulation in red apples. Plant Cell **21:** 168–183.

Fischer, T.C., Mirbeth, B., Rentsch, J., Sutter, C., Ring, L., Flachowsky, H., Habegger, R., Hoffmann, T., Hanke, M.-V., and Schwab, W. (2014). Premature and ectopic anthocyanin formation by silencing of anthocyanidin reductase in strawberry (Fragaria × ananassa). New Phytol. **201:** 440–451.

Forbes-Hernandez, T.Y., Gasparrini, M., Afrin, S., Bompadre, S., Mezzetti, B., Quiles, J.L., Giampieri, F., and Battino, M. (2016). The healthy effects of strawberry polyphenols: Which strategy behind antioxidant capacity? Crit. Rev. Food Sci. Nutr. **56** (Suppl 1): S46–S59.

Gambino, G., Perrone, I., and Gribaudo, I. (2008). A rapid and effective method for RNA extraction from different tissues of grapevine and other woody plants. Phytochem. Anal. **19:** 520–525.

Gao, Q., Luo, H., Li, Y., Liu, Z., and Kang, C. (2020). Genetic modulation of RAP alters fruit coloration in both wild and cultivated strawberry. Plant Biotechnol. J. **18:** 1550–1561.

Gil-Ariza, D.J., Amaya, I., López-Aranda, J.M., Botella, M.A., Valpuesta, V., and Sánchez-Sevilla, J.F. (2009). Impact of plant breeding on the genetic diversity of cultivated strawberry as revealed by expressed sequence tag-derived simple sequence repeat markers. J. Am. Soc. Hortic. Sci. **134:** 337–347.

Garrison, E., and Marth, G. (2012). Haplotype-based variant detection from short-read sequencing. arXiv:1207.3907 [q-bio.GN].

Griesser, M., Hoffmann, T., Bellido, M.L., Rosati, C., Fink, B., Kurtzer, R., Aharoni, A., Muñoz-Blanco, J., and Schwab, W. (2008). Redirection of flavonoid biosynthesis through the down-regulation of an anthocyanidin glucosyltransferase in ripening strawberry fruit. Plant Physiol. **146:** 1528–1539.

Grotewold, E., Drummond, B.J., Bowen, B., and Peterson, T. (1994). The myb-homologous P gene controls phlobaphene pigmentation in maize floral organs by directly activating a flavonoid biosynthetic gene subset. Cell **76:** 543–553.

Hancock, J., Luby, J., Dale, A., Callow, P., Serce, S., and El-Shiek, A. (2002). Utilizing wild Fragaria virginiana in strawberry cultivar development: Inheritance of photoperiod sensitivity, fruit size, gender, female fertility and disease resistance. Euphytica **126:** 177–184.

Hancock, J.F. (1999). Strawberries. (CAB International).

Hancock, J.F., Callow, P.W., Dale, A., Luby, J.J., Finn, C.E., Hokanson, S.C., and Hummer, K.E. (2001). From the Andes to the Rockies: Native strawberry collection and utilization. HortScience **36:** 221–225.

Hancock, J.F., Callow, P.W., Serçe, S., and Son, P.Q. (2003). Variation in the horticultural characteristics of native Fragaria virginiana and F. chiloensis from North and South America. J. Am. Soc. Hortic. Sci. **128:** 201–208.

Harapanhalli, R.S., Howell, R.W., and Rao, D.V. (1993). Testicular and plasma ascorbic acid levels in mice following dietary intake: A high-performance liquid chromatographic analysis. J. Chromatogr. A **614:** 233–243.

Hardigan, M.A., Poorten, T.J., Acharya, C.B., Cole, G.S., Hummer, K.E., Bassil, N., Edger, P.P., and Knapp, S.J. (2018). Domestication of temperate and coastal hybrids with distinct ancestral gene selection in octoploid strawberry. Plant Genome **11:** 1–11.

Hardigan, M.A., Feldmann, M.J., Lorant, A., Bird, K.A., Famula, R., Acharya, C., Cole, G., Edger, P.P., and Knapp, S.J. (2020). Genome synteny has been conserved among the octoploid progenitors of cultivated strawberry over millions of years of evolution. Front Plant Sci **10:** 1789.

Hawkins, C., Caruana, J., Schiksnis, E., and Liu, Z. (2016). Genome-scale DNA variant analysis and functional validation of a SNP underlying yellow fruit color in wild strawberry. Sci. Rep. **6:** 29017.

Härtl, K., Denton, A., Franz-Oberdorf, K., Hoffmann, T., Spornraft, M., Usadel, B., and Schwab, W. (2017). Early metabolic and transcriptional variations in fruit of natural white-fruited Fragaria vesca genotypes. Sci. Rep. **7:** 45113.

He, J., and Giusti, M.M. (2010). Anthocyanins: Natural colorants with health-promoting properties. Annu. Rev. Food Sci. Technol. **1:** 163–187.

Hirsch, C.D., and Springer, N.M. (2017). Transposable element influences on gene expression in plants. Biochim Biophys Acta Gene Regul Mech. **1860:** 157–165.

Hoffmann, T., Kalinowski, G., and Schwab, W. (2006). RNAi-induced silencing of gene expression in strawberry fruit (Fragaria x ananassa) by agroinfiltration: A rapid assay for gene function analysis. Plant J. **48:** 818–826.

Hollender, C.A., Geretz, A.C., Slovin, J.P., and Liu, Z. (2012). Flower and early fruit development in a diploid strawberry, Fragaria vesca. Planta **235:** 1123–1139.

Hollender, C.A., Kang, C., Darwish, O., Geretz, A., Matthews, B.F., Slovin, J., Alkharouf, N., and Liu, Z. (2014). Floral transcriptomes in woodland strawberry uncover developing receptacle and anther gene networks. Plant Physiol. **165:** 1062–1075.

Hossain, M.R., Kim, H.-T., Shanmugam, A., Nath, U.K., Goswami, G., Song, J.-Y., Park, J.-I., and Nou, I.-S. (2018). Expression profiling of regulatory and biosynthetic genes in contrastingly anthocyanin rich strawberry (Fragaria × ananassa) cultivars reveals key genetic determinants of fruit color. Int. J. Mol. Sci. **19:** 656.

Höfgen, R., and Willmitzer, L. (1988). Storage of competent cells for Agrobacterium transformation. Nucleic Acids Res. **16:** 9877.

Jaakola, L. (2013). New insights into the regulation of anthocyanin biosynthesis in fruits. Trends Plant Sci. **18:** 477–483.

Jia, H., Jiu, S., Zhang, C., Wang, C., Tariq, P., Liu, Z., Wang, B., Cui, L., and Fang, J. (2016). Abscisic acid and sucrose regulate tomato and strawberry fruit ripening through the abscisic acid-stress-ripening transcription factor. Plant Biotechnol. J. **14:** 2045–2065.

Jia, H., Wang, Y., Sun, M., Li, B., Han, Y., Zhao, Y., Li, X., Ding, N., Li, C., Ji, W., and Jia, W. (2013). Sucrose functions as a signal involved in the regulation of strawberry fruit development and ripening. New Phytol. **198:** 453–465.

Jia, H.-F., Chai, Y.-M., Li, C.-L., Lu, D., Luo, J.-J., Qin, L., and Shen, Y.-Y. (2011). Abscisic acid plays an important role in the regulation of strawberry fruit ripening. Plant Physiol. **157:** 188–199.

Jian, W., et al. (2019). SlMYB75, an MYB-type transcription factor, promotes anthocyanin accumulation and enhances volatile aroma production in tomato fruits. Hortic. Res. **6:** 22.

Johnson, A.W., Davis, M.J., Grant, O.M., and Simpson, D.W. (2014). Developing Strawberry Cultivars with Improved Water Use Efficiency. Acta Hortic. (1049): 853–858.

Jung, S., Venkatesh, J., Kang, M.-Y., Kwon, J.-K., and Kang, B.-C. (2019). A non-LTR retrotransposon activates anthocyanin biosynthesis by regulating a MYB transcription factor in Capsicum annuum. Plant Sci. **287:** 110181.

Jurka, J. (2013). Repbase Reports 13: 913.

Kadomura-Ishikawa, Y., Miyawaki, K., Takahashi, A., Masuda, T., and Noji, S. (2015). Light and abscisic acid independently regulated FaMYB10 in Fragaria × ananassa fruit. Planta **241:** 953–965.

Kearse, M., et al. (2012). Geneious Basic: An integrated and extendable desktop software platform for the organization and analysis of sequence data. Bioinformatics **28:** 1647–1649.

Kohany, O., Gentles, A.J., Hankus, L., and Jurka, J. (2006). Annotation, submission and screening of repetitive elements in Repbase: RepbaseSubmitter and Censor. BMC Bioinformatics **7:** 474.

Koskela, E.A., Kurokura, T., Toivainen, T., Sønsteby, A., Heide, O.M., Sargent, D.J., Isobe, S., Jaakola, L., Hilmarsson, H., Elomaa, P., and Hytönen, T. (2017). Altered regulation of TERMINAL FLOWER 1 causes the unique vernalisation response in an arctic woodland strawberry accession. New Phytol. **216:** 841–853.

Lerceteau-Köhler, E., Moing, A., Guérin, G., Renaud, C., Petit, A., Rothan, C., and Denoyes, B. (2012). Genetic dissection of fruit quality traits in the octoploid cultivated strawberry highlights the role of homoeo-QTL in their control. Theor. Appl. Genet. **124:** 1059–1077.

Li, H., Handsaker, B., Wysoker, A., Fennell, T., Ruan, J., Homer, N., Marth, G., Abecasis, G., and Durbin, R.; 1000 Genome Project Data Processing Subgroup. (2009). The Sequence Alignment/Map format and SAMtools. Bioinformatics 25: 2078–2079.

Li, Y., Feng, J., Cheng, L., Dai, C., Gao, Q., Liu, Z., and Kang, C. (2019). Gene expression profiling of the shoot meristematic tissues in woodland strawberry Fragaria vesca. Front Plant Sci **10:** 1624.

Li, Y.-Y., Mao, K., Zhao, C., Zhao, X.-Y., Zhang, H.-L., Shu, H.-R., and Hao, Y.-J. (2012). MdCOP1 ubiquitin E3 ligases interact with

MdMYB1 to regulate light-induced anthocyanin biosynthesis and red fruit coloration in apple. Plant Physiol. **160:** 1011–1022.

Lin-Wang, K., Bolitho, K., Grafton, K., Kortstee, A., Karunairetnam, S., McGhie, T.K., Espley, R.V., Hellens, R.P., and Allan, A.C. (2010). An R2R3 MYB transcription factor associated with regulation of the anthocyanin biosynthetic pathway in Rosaceae. BMC Plant Biol. **10:** 50.

Lin-Wang, K., McGhie, T.K., Wang, M., Liu, Y., Warren, B., Storey, R., Espley, R.V., and Allan, A.C. (2014). Engineering the anthocyanin regulatory complex of strawberry (Fragaria vesca). Front Plant Sci **5:** 651.

Liston, A., Cronn, R., and Ashman, T.-L. (2014). Fragaria: A genus with deep historical roots and ripe for evolutionary and ecological insights. Am. J. Bot. **101:** 1686–1699.

Liston, A., Wei, N., Tennessen, J.A., Li, J., Dong, M., and Ashman, T.L. (2020). Revisiting the origin of octoploid strawberry. Nat. Genet. **52:** 2–4.

Liu, X., Huang, M., Fan, B., Buckler, E.S., and Zhang, Z. (2016). Iterative usage of fixed and random effect models for powerful and efficient genome-wide association studies. PLoS Genet. **12:** e1005767.

Lunkenbein, S., Coiner, H., de Vos, C.H.R., Schaart, J.G., Boone, M.J., Krens, F.A., Schwab, W., and Salentijn, E.M.J. (2006). Molecular characterization of a stable antisense chalcone synthase phenotype in strawberry (Fragaria x ananassa). J. Agric. Food Chem. **54:** 2145–2153.

Luo, H., Dai, C., Li, Y., Feng, J., Liu, Z., and Kang, C. (2018). Reduced Anthocyanins in Petioles codes for a GST anthocyanin transporter that is essential for the foliage and fruit coloration in strawberry. J Exp Bot **163:** 2595–2608.

Luo, Y., et al. (2019). ABA and sucrose co-regulate strawberry fruit ripening and show inhibition of glycolysis. Mol. Genet. Genomics **295:** 421–438.

Ma, Z., Zhu, P., Shi, H., Guo, L., Zhang, Q., Chen, Y., Chen, S., Zhang, Z., Peng, J., and Chen, J. (2019). PTC-bearing mRNA elicits a genetic compensation response via Upf3a and COMPASS components. Nature **568:** 259–263.

Marchler-Bauer, A., et al. (2015). CDD: NCBI's conserved domain database. Nucleic Acids Res. **43:** D222–D226.

Martín-Pizarro, C., and Posé, D. (2018). Genome editing as a tool for fruit ripening manipulation. Front Plant Sci **9:** 1415.

McKenna, A., Hanna, M., Banks, E., Sivachenko, A., Cibulskis, K., Kernytsky, A., Garimella, K., Altshuler, D., Gabriel, S., Daly, M., and DePristo, M.A. (2010). The genome analysis toolkit: A Map-Reduce framework for analyzing next-generation DNA sequencing data. Genome Res. **20:** 1297–1303.

Medina-Puche, L., Cumplido-Laso, G., Amil-Ruíz, F., Hoffmann, T., Ring, L., Rodríguez-Franco, A., Caballero, J.L., Schwab, W., Muñoz-Blanco, J., and Blanco-Portales, R. (2014). MYB10 plays a major role in the regulation of flavonoid/phenylpropanoid metabolism during ripening of Fragaria x ananassa fruits. J. Exp. Bot. **65:** 401–417.

Michelmore, R.W., Paran, I., and Kesseli, R.V. (1991). Identification of markers linked to disease-resistance genes by bulked segregant analysis: A rapid method to detect markers in specific genomic regions by using segregating populations. Proc. Natl. Acad. Sci. USA **88:** 9828–9832.

Miosic, S., Thill, J., Milosevic, M., Gosch, C., Pober, S., Molitor, C., Ejaz, S., Rompel, A., Stich, K., and Halbwirth, H. (2014). Dihydroflavonol 4-reductase genes encode enzymes with contrasting substrate specificity and show divergent gene expression profiles in Fragaria species. PLoS One **9:** e112707.

Moyano, E., Portero-Robles, I., Medina-Escobar, N., Valpuesta, V., Muñoz-Blanco, J., and Caballero, J.L. (1998). A fruit-specific putative dihydroflavonol 4-reductase gene is differentially expressed in strawberry during the ripening process. Plant Physiol. **117:** 711–716.

Noh, Y.-H., et al. (2018). High-throughput marker assays for FaRPc2-mediated resistance to Phytophthora crown rot in octoploid strawberry. Mol. Breed. **38:** 1–11.

Notredame, C., Higgins, D.G., and Heringa, J. (2000). T-coffee: A novel method for fast and accurate multiple sequence alignment. In J Mol Biol, Volume **302, pp.** 205–217.

Pellegrini, N., Re, R., Yang, M., and Rice-Evans, C. (1999). Screening of dietary carotenoids and carotenoid-rich fruit extracts for antioxidant activities applying 2, 2′-azinobis (3-ethylenebenzothiazoline-6-sulfonic acid radical cation decolorization assay. Methods Enzymol. **299:** 379–389.

Re, R., Pellegrini, N., Proteggente, A., Pannala, A., Yang, M., and Rice-Evans, C. (1999). Antioxidant activity applying an improved ABTS radical cation decolorization assay. Free Radic. Biol. Med. **26:** 1231–1237.

Rebollo, R., Romanish, M.T., and Mager, D.L. (2012). Transposable elements: An abundant and natural source of regulatory sequences for host genes. Annu. Rev. Genet. **46:** 21–42.

Sablowski, R.W., Moyano, E., Culianez-Macia, F.A., Schuch, W., Martin, C., and Bevan, M. (1994). A flower-specific Myb protein activates transcription of phenylpropanoid biosynthetic genes. EMBO J. **13:** 128–137.

Salvatierra, A., Pimentel, P., Moya-León, M.A., Caligari, P.D.S., and Herrera, R. (2010). Comparison of transcriptional profiles of flavonoid genes and anthocyanin contents during fruit development of two botanical forms of Fragaria chiloensis ssp. chiloensis. Phytochemistry **71:** 1839–1847.

Salvatierra, A., Pimentel, P., Moya-León, M.A., and Herrera, R. (2013). Increased accumulation of anthocyanins in Fragaria chiloensis fruits by transient suppression of FcMYB1 gene. Phytochemistry **90:** 25–36.

Sánchez-Sevilla, J.F., Horvath, A., Botella, M.A., Gaston, A., Folta, K., Kilian, A., Denoyes, B., and Amaya, I. (2015). Diversity Arrays Technology (DArT) marker platforms for diversity analysis and linkage mapping in a complex crop, the octoploid cultivated strawberry (Fragaria × ananassa). PLoS One **10:** e0144960.

Sánchez-Sevilla, J.F., Vallarino, J.G., Osorio, S., Bombarely, A., Posé, D., Merchante, C., Botella, M.A., Amaya, I., and Valpuesta, V. (2017). Gene expression atlas of fruit ripening and transcriptome assembly from RNA-seq data in octoploid strawberry (Fragaria × ananassa). Sci. Rep. **7:** 13737.

Semagn, K., Babu, R., Hearne, S., and Olsen, M. (2013). Single nucleotide polymorphism genotyping using Kompetitive Allele Specific PCR (KASP): Overview of the technology and its application in crop improvement. Mol. Breed. **33:** 1–14.

Shulaev, V., et al. (2011). The genome of woodland strawberry (Fragaria vesca). Nat. Genet. **43:** 109–116.

Staudt, G. (1999). Systematics and Geographic Distribution of the American Strawberry Species. (Univ of California Press).

Staudt, G.S. (2009). Strawberry biogeography, genetics and systematics. Acta Hortic. 71–84.

Stracke, R., Werber, M., and Weisshaar, B. (2001). The R2R3-MYB gene family in Arabidopsis thaliana. Curr. Opin. Plant Biol. **4:** 447–456.

Takagi, H., et al. (2013). QTL-seq: Rapid mapping of quantitative trait loci in rice by whole genome resequencing of DNA from two bulked populations. Plant J. **74:** 174–183.

Tang, Y., Liu, X., Wang, J., Li, M., Wang, Q., Tian, F., Su, Z., Pan, Y., Liu, D., Lipka, A.E., Buckler, E.S., and Zhang, Z. (2016). GAPIT Version 2: An enhanced integrated tool for genomic association and prediction. Plant Genome **9**.

Team, R.C. (2014). R: A language and environment for statistical computing. R foundation for statistical computing. (Austria: Viena).

Tennessen, J.A., Govindarajulu, R., Ashman, T.-L., and Liston, A. (2014). Evolutionary origins and dynamics of octoploid strawberry subgenomes revealed by dense targeted capture linkage maps. Genome Biol. Evol. **6**: 3295–3313.

Thill, J., Miosic, S., Gotame, T.P., Mikulic-Petkovsek, M., Gosch, C., Veberic, R., Preuss, A., Schwab, W., Stampar, F., Stich, K., and Halbwirth, H. (2013). Differential expression of flavonoid 3′-hydroxylase during fruit development establishes the different B-ring hydroxylation patterns of flavonoids in Fragaria × ananassa and Fragaria vesca. Plant Physiol. Biochem. **72**: 72–78.

Tohge, T., de Souza, L.P., and Fernie, A.R. (2017). Current understanding of the pathways of flavonoid biosynthesis in model and crop plants. J. Exp. Bot. **68**: 4013–4028.

Trapnell, C., Roberts, A., Goff, L., Pertea, G., Kim, D., Kelley, D.R., Pimentel, H., Salzberg, S.L., Rinn, J.L., and Pachter, L. (2012). Differential gene and transcript expression analysis of RNA-seq experiments with TopHat and Cufflinks. Nat. Protoc. **7**: 562–578.

Turner, S.D. (2014). qqman: An R package for visualizing GWAS results using Q-Q and manhattan plots. J Open Source Softw **3**: 731.

Vallarino, J.G., de Abreu E Lima, F., Soria, C., Tong, H., Pott, D.M., Willmitzer, L., Fernie, A.R., Nikoloski, Z., and Osorio, S. (2018). Genetic diversity of strawberry germplasm using metabolomic biomarkers. Sci. Rep. **8**: 14386.

van Ooijen, J.W. (2009). MapQTL 6: Software for the mapping of quantitative trait loci in experimental populations of diploid species. (Wageningen, The Netherlands: Kyazma B. V.).

van Ooijen, J.W. (2006). JoinMap4; Software for the calculation of genetic linkage maps in experimental populations. (Wageningen: Kyazma BV).

Vicient, C.M., and Casacuberta, J.M. (2017). Impact of transposable elements on polyploid plant genomes. Ann. Bot. **120**: 195–207.

Voinnet, O., Rivas, S., Mestre, P., and Baulcombe, D. (2003). An enhanced transient expression system in plants based on suppression of gene silencing by the p19 protein of tomato bushy stunt virus (erratum Plant J. 2015 Aug;83(4):752). Plant J. **33**: 949–956.

Voorrips, R.E. (2002). MapChart: Software for the graphical presentation of linkage maps and QTLs. J. Hered. **93**: 77–78.

Wang, H., et al. (2020). The control of red colour by a family of MYB transcription factors in octoploid strawberry (Fragaria × ananassa) fruits. Plant Biotechnol. J. **18**: 1169–1184.

Whitaker, V.M., et al. (2020). A roadmap for research in octoploid strawberry. Hortic. Res **7**: 33.

Williamson, S.C., Yu, H., and Davis, T.M. (1995). Shikimate dehydrogenase allozymes: Inheritance and close linkage to fruit color in the diploid strawberry. J. Hered. **86**: 74–76.

Wittwer, C.T., Reed, G.H., Gundry, C.N., Vandersteen, J.G., and Pryor, R.J. (2003). High-resolution genotyping by amplicon melting analysis using LCGreen. Clin. Chem. **49**: 853–860.

Xu, W., Dubos, C., and Lepiniec, L. (2015). Transcriptional control of flavonoid biosynthesis by MYB-bHLH-WDR complexes. Trends Plant Sci. **20**: 176–185.

Yan, C., An, G., Zhu, T., Zhang, W., Zhang, L., Peng, L., Chen, J., and Kuang, H. (2019). Independent activation of the BoMYB2 gene leading to purple traits in Brassica oleracea. Theor. Appl. Genet. **132**: 895–906.

Zhang, L., et al. (2019). A high-quality apple genome assembly reveals the association of a retrotransposon and red fruit colour. Nat. Commun. **10**: 1494–13.

Zhang, Y., Butelli, E., and Martin, C. (2014). Engineering anthocyanin biosynthesis in plants. Curr. Opin. Plant Biol. **19**: 81–90.

Zhang, Y., Li, W., Dou, Y., Zhang, J., Jiang, G., Miao, L., Han, G., Liu, Y., Li, H., and Zhang, Z. (2015). Transcript quantification by RNA-seq reveals differentially expressed genes in the red and yellow fruits of Fragaria vesca. PLoS One **10**: e0144356.

Zhou, J., Wang, G., and Liu, Z. (2018). Efficient genome editing of wild strawberry genes, vector development and validation. Plant Biotechnol. J. **16**: 1868–1877.

Zorrilla-Fontanesi, Y., Cabeza, A., Domínguez, P., Medina, J.J., Valpuesta, V., Denoyes-Rothan, B., Sánchez-Sevilla, J.F., and Amaya, I. (2011). Quantitative trait loci and underlying candidate genes controlling agronomical and fruit quality traits in octoploid strawberry (Fragaria × ananassa). Theor. Appl. Genet. **123**: 755–778.